New Jersey Institute of Technology

Digital Commons @ NJIT

8-30-2019

Enzymatic biofuel cells in a sandwich geometry with compressed carbon nanotubes/enzyme electrodes & hybrid patch applications

Biao Leng
New Jersey Institute of Technology

Recommended Citation

ABSTRACT

ENZYMATIC BIOFUEL CELLS IN A SANDWICH GEOMETRY WITH COMPRESSED CARBON NANOTUBES/ENZYME ELECTRODES & HYBRID PATCH APPLICATIONS

by
Biao Leng

Enzymatic biofuel cells (EBFCs) convert the chemical energy of biofuels, such as glucose and methanol, into electrical energy by employing enzymes as catalysts. In contrast to conventional fuel cells, EBFCs have a simple membrane-free fuel cell design due to the high catalytic specificity of the enzymes, but the power densities obtained are lower. Although the primary goal of research on EBFCs has been to develop a sustainable power source that can be directly implanted in the human body to power bio-devices, other applications such as the use of a flexible film or fuel cell patch as a wearable power source and sensor, are emerging. The power density and lifetimes of early EBFCs were not promising due to the difficulty of transporting electrons from reactive sites to the electrodes and the tendency of enzymes to migrate away from the electrodes. In recent years, direct electron transport *via* highly conducting functionalized multiwall carbon nanotubes has been demonstrated to be an effective solution. Further improvements can be made with enzyme immobilization during the procedure of bio-electrode fabrication.

This doctoral dissertation focuses on current problems of EBFCs involving immobilization of enzymes, and optimization of the performance of the cells. The technique of immobilization of enzymes, used in this dissertation, is hydraulic pressure to stabilize the enzymes on the electrodes. A novel design of EBFC in sandwich geometry with multiple configuration has been proposed, fabricated and tested. The performance tests of the samples

have been conducted and presented by analyzing the polarization curves and power density versus time. Comparisons have been made to find the integrity/best performance of different configurations. The utility of the hybrid patch configuration and multiple units in series as a stack have been examined in accord with the protocol. A significant increase in power density has been observed for the hybrid EBFC patch units in series. The potential for commercialization and mass production of EBFC applications has been discussed. The preliminary results of the investigation of biofuel cell mechanisms by Surface-Enhancement Raman Spectroscopy (SERS) measurements is presented in the Appendix. With the combination of the usage of both Field Emission SEM and SERS, evidence of the existence of hydrogen peroxide can be verified. H_2O_2 plays an important role in the loss of power in EBFC samples.

The research in this dissertation will shed important light on the development of EBFC research and pave the way for viable commercialization applications.

ENZYMATIC BIOFUEL CELLS IN A SANDWICH GEOMETRY WITH COMPRESSED CARBON NANOTUBES/ENZYME ELECTRODES & HYBRID PATCH APPLICATIONS

by
Biao Leng

A Dissertation
Submitted to the Faculty of
New Jersey Institute of Technology
in Partial Fulfillment of the Requirements for the Degree of
Doctor of Philosophy in Materials Science and Engineering

Interdisciplinary Program in Materials Science and Engineering

August 2019

APPROVAL PAGE

ENZYMATIC BIOFUEL CELLS IN A SANDWICH GEOMETRY WITH COMPRESSED CARBON NANOTUBES/ENZYME ELECTRODES & HYBRID PATCH APPLICATIONS

Biao Leng

Dr. Zafar Iqbal, Dissertation Co-Advisor   Date
Research Professor, Department of Chemistry and Environmental Science, NJIT

Dr. Nuggehalli M Ravindra, Dissertation Co-Advisor   Date
Professor, Materials Science and Engineering Program, NJIT

Dr. Andrei Sirenko, Committee Member   Date
Professor and Chair, Department of Physics, NJIT

Dr. Kamalesh K. Sirkar, Committee Member   Date
Distinguished Professor, Department of Chemical and Materials Engineering, NJIT

Dr. Michael Jaffe, Committee Member   Date
Research Professor, Department of Biomedical Engineering, NJIT

BIOGRAPHICAL SKETCH

Author: Biao Leng

Degree: Doctor of Philosophy

Date: August 2019

Undergraduate and Graduate Education:

- Ph.D. in Materials Science and Engineering,
  New Jersey Institute of Technology, Newark, NJ, 2019

- Master of Science in Materials Science and Engineering,
  New Jersey Institute of Technology, Newark, NJ, 2015

- Bachelor of Science in Applied Physics,
  Sichuan University, Chengdu, People's Republic of China, 2013

Major: Materials Science and Engineering

Presentations and Publications:

Laila, A.; Biao L., "Gold Nanoparticles Assembled on Multilayer Graphene Sheets for Surface-Enhanced Raman Spectroscopy of Glucose," Materials Research Society, Boston, MA, November 2017.

Laila, A.; Biao L., "Surface-enhanced Raman detection of glucose on different substrates for biosensing applications," Materials Science& Technology, Columbus, OH, October 2018.

Biao L.; Laila, A., "Biofuel cells with pressure-immobilized enzymes on carbon nanotube sheets," Materials Science& Technology, Columbus, OH, October 2018.

Biao L, Qin Z et al., "A "Press and Go" Thin Biofuel Cell Patch for Power Generation," JOM - The Journal of The Minerals, Metals & Materials Society, pp. 1-5, June 2019.

This dissertation is dedicated to my parents Yunfei Leng and Honglian Yi and my wife Xiaotang Ma; it was their support that gave me the ability to complete this work.

感恩我的父母冷云飞和易红联对我长久以来的支持与鼓励，感恩我的妻子马晓棠对我的关怀与信任。路漫漫其修远兮 吾将上下而求索！

ACKNOWLEDGMENT

I would like to thank my committee members: Dr. Andrei Sirenko, Dr. Kamalesh K. Sirkar and Dr. Michael Jaffe for their insight and suggestions.

I would like to thank my PhD advisors Dr. Zafar Iqbal and Dr. Nuggehalli M. Ravindra for their great kindness and support. I would like to thank the Department of Physics for the financial support. I express my heart-felt gratitude to Dr. Laila Alqarni; it would be significantly more difficult without her scientific input and personal help to complete my experiments.

I would also like to thank my wife Xiaotang Ma and my parents Yunfei Leng and Honglian Yi for their love, their support is my greatest motivation.

TABLE OF CONTENTS

TABLE OF CONTENTS
(Continued)

LIST OF TABLES

LIST OF FIGURES

CHAPTER 1

INTRODUCTION

1.1 General Background

In recent decades, the world energy consumption continues to be on the rise. According to *BP Statistical Review of World Energy 2018,* the world primary energy consumption grew by 2.2% in 2017 compared to 1.2% in 2016, and it is the highest since 2013 (Figure 1.1). The renewable energy consumption in 2017 was 486.8/13511.2 Million tons oil equivalent, which is 3.6% of the total energy consumption for the year[1]. The major sources of energy are coal, oil and natural gas, which are fossil fuels. Ever since the discovery of fossil fuels in the 18th century, it remains the primary energy source. After centuries of usage of fossil fuels, its aftermath, global warming, has become much more severe; this includes, for example, the increasingly destructive power and numbers per year of hurricanes. In order to slow down global warming, increasing the proportional use of alternative energy sources in the world energy consumption has become an urgent issue.

World consumption
Million tonnes oil equivalent

- Coal
- Renewables
- Hydroelectricity
- Nuclear energy
- Natural gas
- Oil
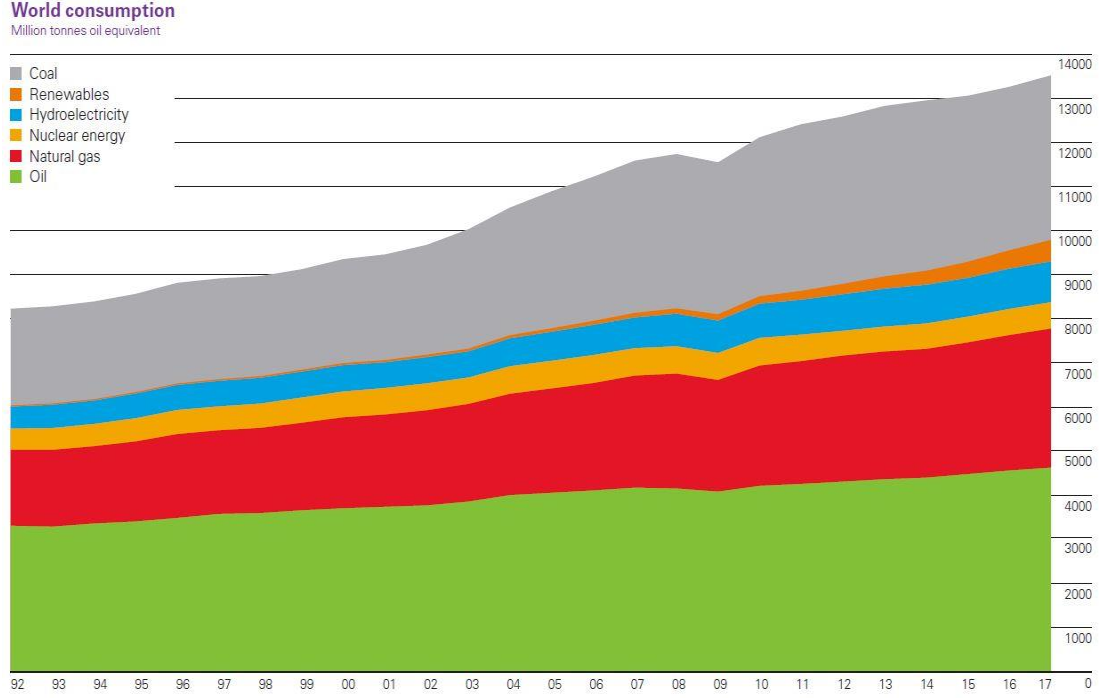
Figure 1.1 World energy consumption from 1992 to 2017 [1].

In order to mitigate this issue, numerous scientists and engineers have been working on developing many different alternative energy sources. Fuel cells, a promised concept, is among them. A fuel cell is a device that generates electrical power from a chemical source, such as hydrogen in a hydrogen fuel cell that converts chemical energy via the electrochemical reaction of the hydrogen fuel with oxygen from an oxidizing agent. Typically, the chemical reaction is as follows:

$$2H_2 \rightarrow 4H^+ + 4e^- \qquad\qquad (1.1)$$

$$O_2 + 4H^+ + 4e^- \rightarrow 2H_2O \qquad\qquad (1.2)$$

$$2H_2 + O_2 \rightarrow 2H_2O \qquad\qquad (1.3)$$
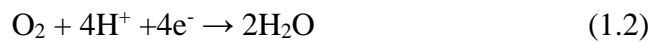
Equation 1.1 is for the anode, Equation 1.2 is for the cathode and Equation 1.3 is the overall equation. Compared to a fossil energy source such as petroleum, fuel cells are a clean power source for automobiles. There are no emissions of polluting gases,

2

such as NO_x, SO_x and CO – the only emission is that of water vapor produced by the reaction (1.3) above. The first fuel cell was invented by William Grove in 1838 [2]. The first commercialized fuel cell was developed by the General Electric Company in the1950s. More and more attention has been given to this technology and today, for example, there are three brands of all hydrogen fuel cell electric cars – Hyundai's Nexo, Toyota's Mirai and Honda's Clarity. The advantage of fuel cell cars compared with all-electric battery cars like the Tesla, is that filling up with hydrogen is comparable to that of gasoline powered cars and can be completed in a few minutes, whereas the typical charging time for Tesla is of the order of 30 minutes or more. On the other hand, hydrogen fueling stations are scarce and at this time, they are to be found only in the state of California in the United States. Also, as pointed out by Elon Musk, Tesla's founder among others, producing hydrogen currently involves the breaking down of natural gas using a process with carbon emission that is not green. Before a hydrogen economy becomes a reality, infrastructure and hydrogen production/storage issues have to be resolved and are being currently addressed by the US Department of Energy.

Typical Fuel Cell (FC) designs include (Figure 1.2):

- Anode, where typically platinum is used as the catalyst to oxidize hydrogen into protons and electrons according to reaction (1.1).
- Cathode, where the oxygen reduction [reaction (1.2)], also typically catalyzed by platinum, occurs to convert protons and oxygen into water [reaction (1.3)].
- Electrolyte, which is the medium where protons and oxygen react to form water. Different types of FCs have different electrolyte substances; for example, potassium hydroxide, phosphoric acid and yttria-stabilized zirconia[3].
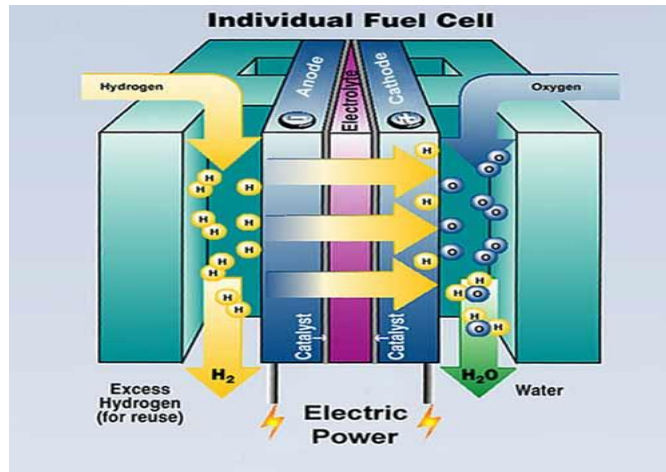
Figure 1.2 Schematic diagram showing the operation of a hydrogen fuel cell [4].

Fuel cells can be classified into different types (see Table 1.1) according to the electrolyte used. For example, potassium hydroxide solution infiltrated into a porous membrane is used in an alkaline fuel cell (AFC); polymer membranes, such as Nafion®, are used in proton exchange membrane fuel cells (PEMFC); phosphoric acid aqueous electrolyte is used in phosphoric acid fuel cell (PAFC); molten lithium carbonate and potassium carbonate are used in molten carbonate fuel cell (MCFC), and zirconium oxide with yittrium oxide is used in solid oxide fuel cell (SOFC).

Table 1.1 Examples of Different Types of Fuel Cells [5]

	AFC	PEMFC	PAFC	MCFC	SOFC
Tempereture (°C)	60 - 90	80 - 110	160 - 200	600 - 800	800 - 1000
Electrode material	Metal or carbon	Pt-on carbon	Pt-on carbon	Ni + Cr	Ni / Y_2O_3-ZrO_2
Electrolyte	NaOH/KOH	Polymer membrane	H_3PO_4	$LiCO_3$-K_2 CO_3	ZrO_2 with $Y2O_3$
Primary fuel	H_2	H_2 reformate	H_2 reformate	H_2 / CO reformate	H_2 / CO / CH_4 reformate
Oxidant	O_2 / air	O_2 / air	O_2 / air	CO_2 / O_2 / air	O_2 / air
Issues	CO_2 troubles	Moisture of fuel	CO sensitivity	CO_2 recycling necessary	Ceramic cells
Practical efficiency (%)	60	60	55	55-65[a]	60-65[a]

Another type of fuel cell, different from those described above, is the biofuel fuel cell (BFC). BFCs use biocatalysts, such as enzymes, and organics, typically glucose and methanol as the electrolyte and fuel. For this reason, BFCs can operate at room temperature.

1.2 Biofuel Cells

Biofuel cells or biological fuel cells are a special type of fuel cells. In principle, they work in the same way as a conventional hydrogen fuel cell. The fuel and oxidant react at the electrodes to generate electrical power via electrons formed at the anode. In biofuel cells, the fuel is a hydrocarbon, such as glucose or an alcohol instead of hydrogen. For example, the anodic reaction for a biofuel cell using glucose as the fuel is given by:

$$C_6H_{12}O_6 + 6H_2O \rightarrow 6CO_2 + 24H^+ + 24e^- \tag{1.4}$$
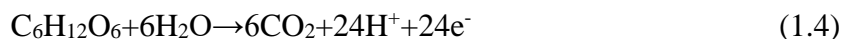
and the cathode reaction, where oxygen is reduced by the electrons produced at the anode, is given by:

$$6O_2 + 24H^+ + 24e^- \rightarrow 12H_2O \tag{1.5}$$
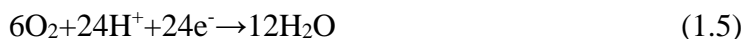
The electrons formed at the anode pass through an external circuit to produce an electric current and generate power.

Biofuel cells use living bacteria or enzymes to catalyze the redox reactions as in reactions 1.4 and 1.5 and organic matter as fuel. There are thus two categories of biofuel cells, Microbial Fuel Cells (MFC) which are catalyzed by living bacteria and Enzymatic Biofuel Cells (EBFC) where enzymes function as the catalyst.

1.2.1 Microbial Fuel Cells

An MFC is a device that generates electrical energy by the action of active microorganisms[6]. Most MFCs have the same configuration of anode and cathode chamber which are separated by a Proton Exchange Membrane (PEM). The oxidation of organic carbon sources or substrates takes place on the anode by the active biocatalyst and reduction process takes place on the cathode. During the oxidation process, electrons and protons are produced. The electrons are transferred to an electrode while the protons are transferred through the PEM to the cathode chamber. Then the protons react with electrons and oxygen at the cathode to produce water[7]. For example, the reaction of acetic acid on the anode and oxygen on the cathode, are given in Equations 1.6 and 1.7, respectively.

$$C_2H_4O_2 + 2H_2O \rightarrow 2CO_2 + 8e^- + 8H^+ \qquad\qquad (1.6)$$

$$2O_2 + 8H^+ + 8e^- \rightarrow 4H_2O \qquad\qquad (1.7)$$
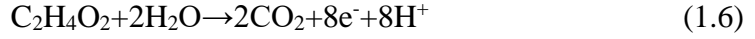
Although the first observation of bacteria producing electrical current was made by Potter in 1911 [8], very limited improvements were made only in the early 1990s [6].
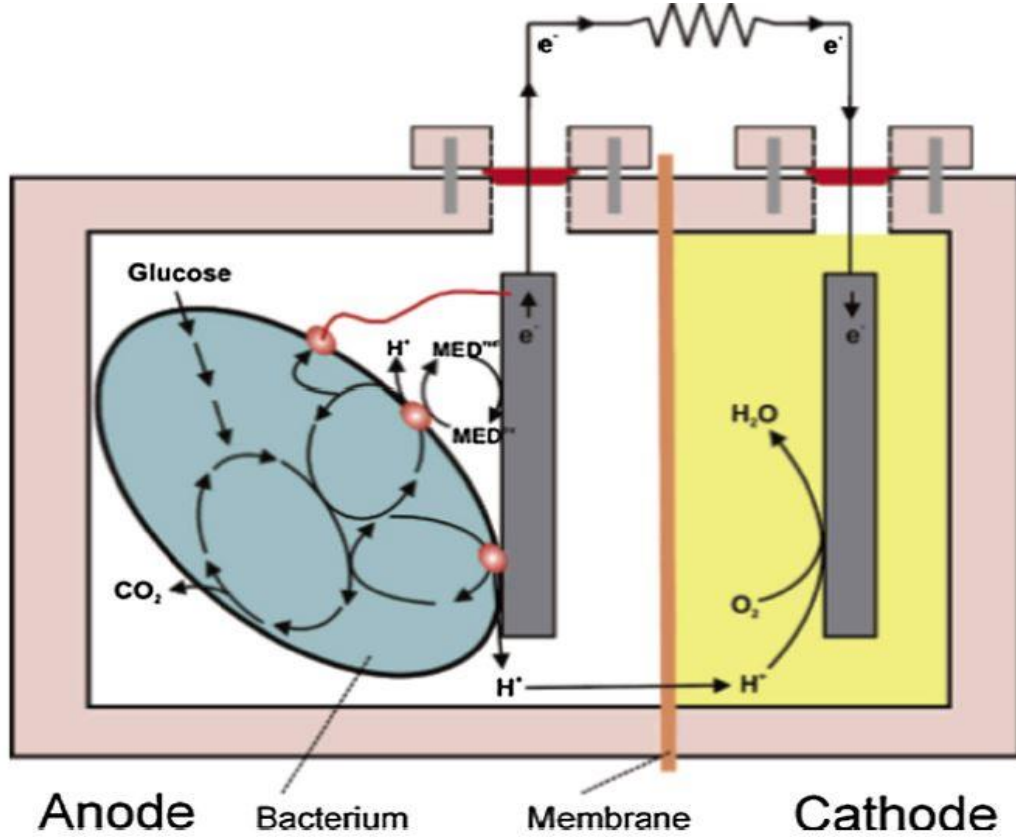
Figure 1.3 Schematic diagram showing the operation of a microbial fuel cell [9]

Typically, the design of an MFC consists of anode and cathode chambers which are separated by a proton exchange membrane (Figure 1.3). Bacteria at the anode chamber functions as the catalyst to produce protons and electrons. Then the electrons are transferred to the anode via a mediator. The cathode chamber is where the protons

react with oxygen to form water. The cathode materials are mostly carbon based materials, such as carbon fiber felt, graphite felt and platinum coated carbon paper.

There are various factors affecting the performance of MFCs such as electrode materials, permeability of proton exchange membrane, the transfer rate of electrons to anode via mediator and so forth[9].

Table 1.2 Some Examples of MFCs and their Performance

Bacteria	Anode	Substrate	Maximum power density (mW/m^2)	Refs.
Deltaproteo bacterium	Graphite	Marine sediment reached in acetate	14	[10]
Saccharomyces cerevisiae	Graphite	Glucose	16	[11]
Gammaproteo and shewanellaaffinis (KMM3586)	Carbon paper	Cyctenin	36	[12]
Escherichia coli	Graphite with Mn^{4+}	Sewage sludge	91	[13]
Escherichia coli	Composite electrode (graphite/PTFE)	Glucose	760	[7]
Escherichia coli	Carbon paper with PPY-CNTs modified	Glucose	228	[14]

For different bacteria, they require different substrates as the fuel. Table 1.2 shows some example of the types of bacteria, anode materials, and substrates that are used for the MFCs and the power density obtained from them.

The advantage of using bacteria as the catalyst is that it does not require expensive metal as catalyst, and the operating temperature normally is room temperature. MFCs also have great potential for waste water treatment.

However, the power output is very limited for MFCs. The proton exchange

membrane is the main source of internal resistance restricting the power output of MFCs[15].

1.2.2 Enzymatic Biofuel Cells

The general idea of enzymatic biofuel cells (EBFCs) is that they converts the chemical energy of some specific biofuels such as glucose and alcohol into electrical energy by employing the enzymes as catalysts on the electrodes. The biofuels used in the process need to be specific; this is because of the specificity of enzymes; they are specific for a particular type of chemical bond or functional group. Different from the MFCs, EBFCs use enzyme proteins instead of bacteria as catalysts. Some examples of the these enzymes are Glucose Oxidase (GOx), Bilirubin Oxidase and Laccase (Lac). The enzyme catalysts cause the biofuel to undergo redox reactions while the electrons are transferred from the anode to the cathode via an external circuit to generate power (Figure 1.4).
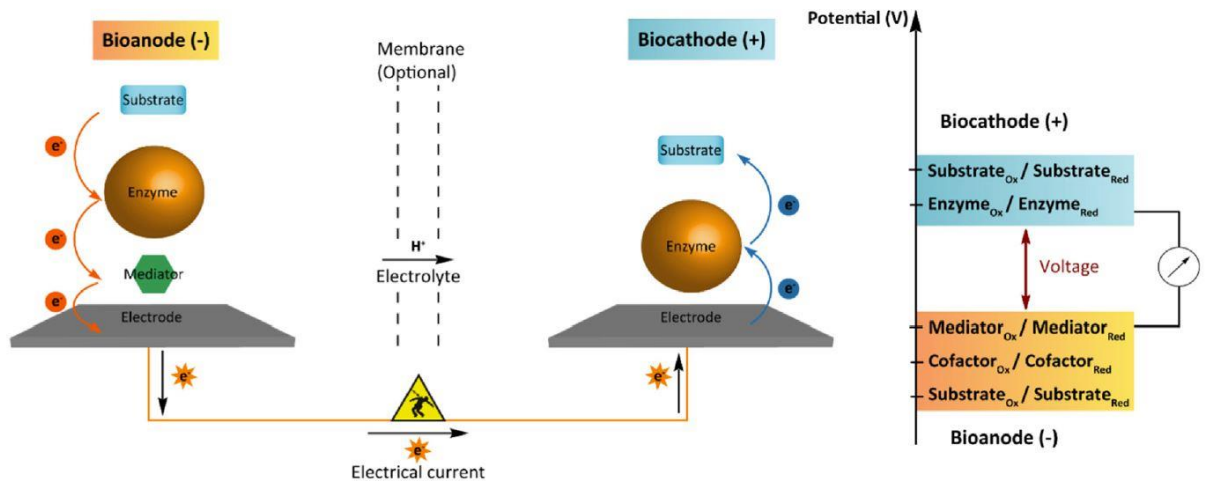
Figure 1.4 Schematic representation for an EBFC [16]

Compared to conventional fuel cells, EBFC has some advantages, such as a simple

fuel cell design and lower cost of the main fuel cell components; for instance, it does not require expensive metal platinum to construct electrodes. The first working enzymatic biofuel cell was produced in 1964; it used GOx bioanode and a Pt cathode [17]. The open circuit potentials of this EBFC was very low (175-350mV), but it established a proof of concept of a working EBFC device. Similar to MFCs, this design also reqired a mediator for the transfer of electrons from the active site/cofactor to the electrode surface. This electron transfer system is referred to as mediated electron transfer (MET). Mediators can shorten the distance between the redox center of certain enzyme and electrode surface for the electron transfer based on a diffusional mechanism [18].

To ensure an efficient electrical communication between the active site and electrodes, a small redox active molecule which has similar redox potential as the active center of the enzyme is required. In 1978, Berezin et al. discovered a new electron transfer method involving direct electron transfer (DET) [19]. Different from MET, DET does not use an external redox mediator; it can transfer electrons directly from the active site/cofactor in the enzyme protein to the electrode. Without the usage of a mediator, the electric potential in EBFCs is higher than those with MET system and there is no more stability issue of the mediator. Even though, theoretically, MET systems can cause potential loss and lack of stability, they were used by most of the reaserchers in the early days because they usually have higher current densities [20, 21]. Figure 1.5 shows schematics of MET and DET.
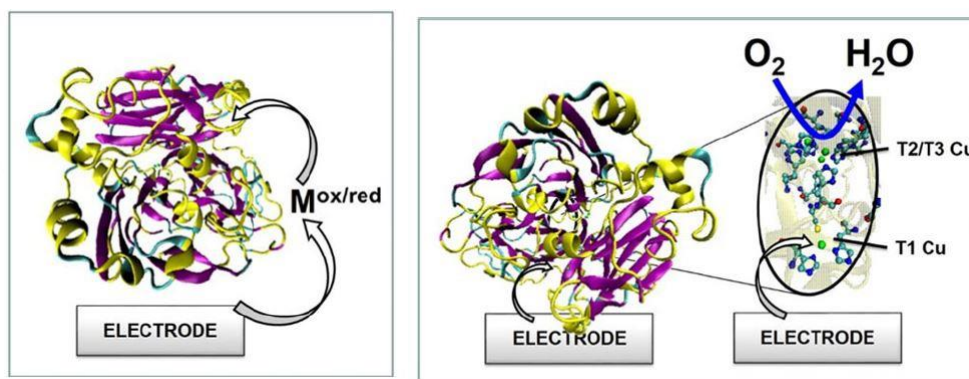
Figure 1.5 Electrons can be transferred via MET (left) and DET(right) [22]

The redox enzymes are essential to the electrochemical reactions. Even though all these enzymes serve as the catalyst for the reactions, they are not all the same. The active centers and locations can be different regarding the types of enzyme, which lead to the reason of different electron transfer mechanism.

Some enzymes have nicotinamide adenine dinucleotide (NADH/NAD+) or nicotinamide adenine dinucleotide phosphate (NADPH/NADP+) as their redox centers. The redox centers of these type of enzymes are often weakly bound to the main body of the enzyme protein. Examples are Glucose dehydrogenase (GDH) and alcohol dehydrogenase. Some enzymes have a redox center that is located near the edge of the protein shell such as laccase and peroxidases. Due to the conveniently located redox center, it allows electrons to transfer directly between the active redox center and the electrode surface.
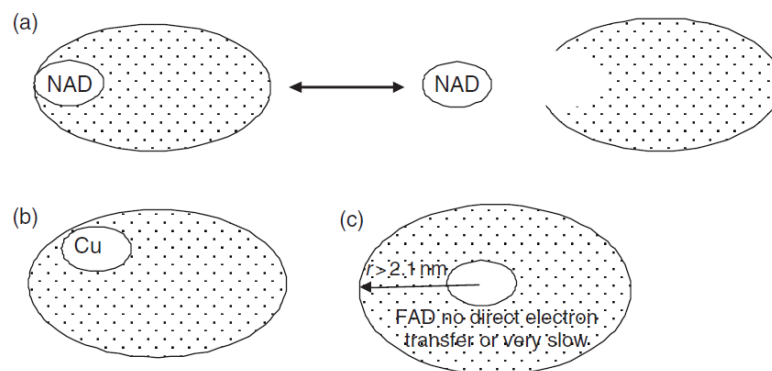
Figure 1.6 The location of enzyme active center. (a) Diffusive active center, (b) active center on or near the edge of the enzyme protein shell, and (c) strongly bound and deep-buried redox centers [23]

There are some other enzymes which have a relatively deep and strongly bonded redox center in the protein shell, for exmaple GOx[24]. It is difficult for such kind of an enzyme to have DET between the active site and electrodes due to the large distance, normally over 21Å[25]. In this case, MET is mostly used.

Anode
Glucose + GOx[ox] →
        GOx[red] + glucolactone + 2H$^+$
GOx[red] + mediator[ox] →
        mediator[red] + GOx[ox]
Mediator[red] →
        mediator[ox] + 2e$^-$ (to anode)

Glucose →
        glucolactone + 2H$^+$ + 2e$^-$
Glucolactone + H$_2$O → gluconic acid

Cathode
Multicopper oxidases + 1/2O$_2$ + 2e$^-$ + 2H$^+$
→ H$_2$O
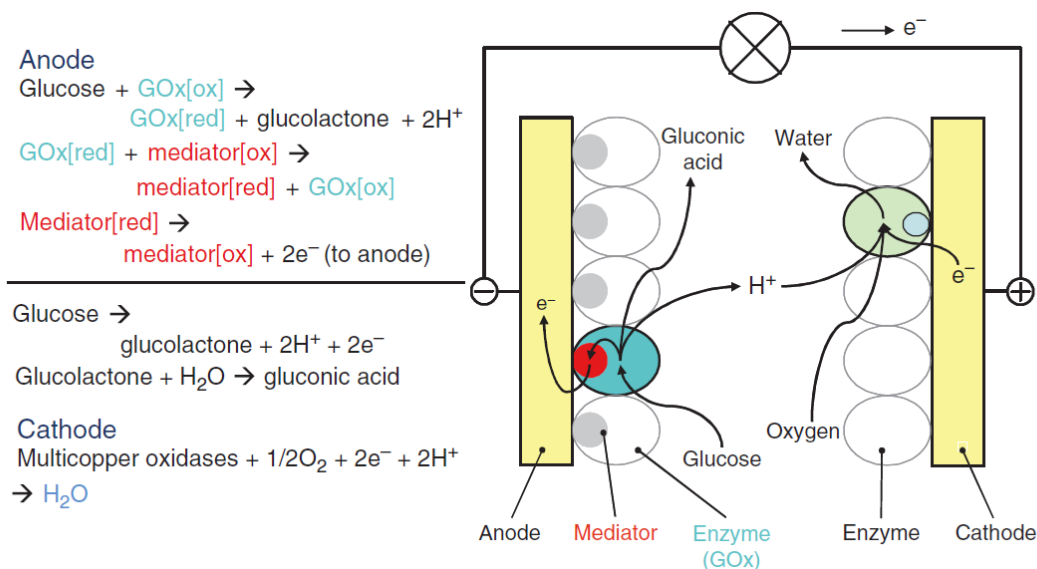
Figure 1.7 Schematic diagram of MET in a GOx-based EBFC [23].

Mediators such as ferrocene derivatives [26], hydroquinone [27], benzoquinone [28], and pyrroloquinoline quinone (PQQ) [29] have been reported to be appropriate for GOx. Equations 1.8−1.10 show the anodic reactions of an EBFC developed by Katz and Willner using PQQ as mediator[30]. Flavin adenine dinucleotide (FAD) is the cofactor that is in the GOx redox center[24, 30-32]. Two electrons were generated while the glucose was oxidized by GOx producing gluconic acid. The FAD was reduced into $FADH_2$ after it accepts the $2e^-$(Reaction 1.8). Then the $FADH_2$ was oxidized and recovered into FAD by PQQ releasing $2e^-$ and hydrogen, while the PQQ became $PQQH_2$ (Reaction 1.9). Later, the $PQQH_2$ was futher oxidized back to PQQ around the electrode, releasing $2e^-$ and $2H^+$ (Reaction 1.10).

Electrode−PQQ−FAD–Gox + Glucose $\rightarrow$ Electrode−PQQ−$FADH_2$−GOx +Gluconic acid   (1.8)

Electrode−PQQ−$FADH_2$−GOx $\rightarrow$ Electrode−$PQQH_2$−FAD−GOx   (1.9)

Electrode−$PQQH_2$−FAD−GOx $\rightarrow$ Electrode−PQQ−FAD−GOx + $2H^+$ + $2e^-$ (1.10)
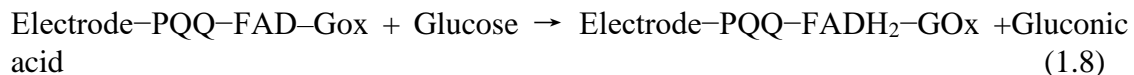
In recent years, carbon nanotubes (CNTs) have become a topic of significant interest in fabricating electrodes for EBFCs due to their excellent stability, biocompatibility and high electrical conductivity. The CNTs, with diameters ranging from 1 nm (SWCNTs) to 10 nm (MWCNTs), were widely used for applications in EBFCs. This is because CNT allows EBFCs to be in close proximity to the active sites of enzymes for more efficient electron transfer rate. Additional details of this methodology will be discussed in the section on carbon nanotubes. With the introduction of CNTs in fabricating bioelectrode, it allows EBFCs that use DET to exhibit better performance than those with MET. For example, glucose enzymatic biofuel cell is one

kind of EBFC which uses glucose as fuel, generally glucose oxidase (GOx) and laccase

as anode and cathode catalyst, respectively. The reaction is as follows:

$$\text{Glucose} + \text{FAD-GOx} \rightarrow \text{gluconolactone} + \text{FADH}_2\text{-GOx} \qquad (1.11)$$

$$\text{FADH}_2\text{-GOx} + \text{O}_2 \rightarrow \text{FAD-GOx} + \text{H}_2\text{O}_2 \qquad (1.12)$$
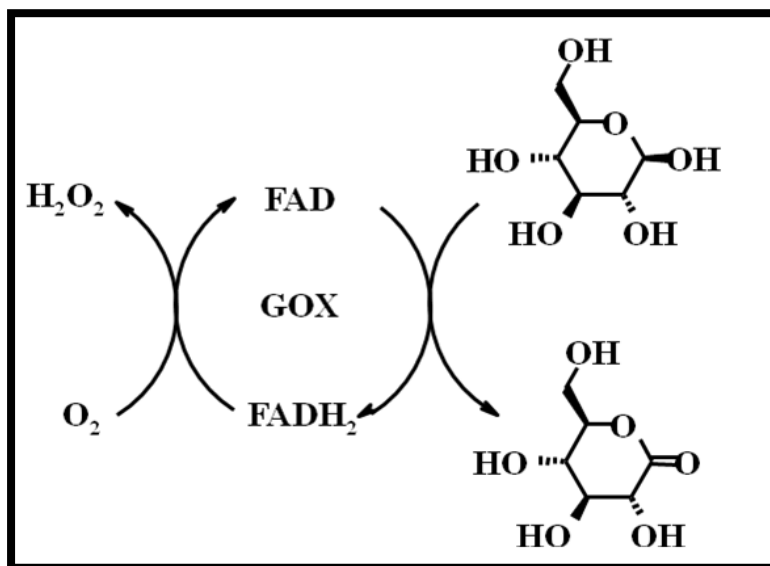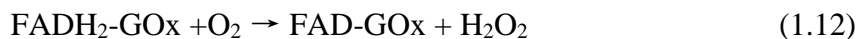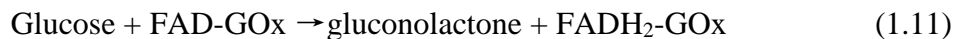
Figure 1.8 Mechanism of oxidation process of cofactor FAD in GOx[33].

Biocatalysts provide a variety of advantages over the regular metal catalysts since

they are highly selective, active under mild conditions, (neutral pH, and body

temperature) and are highly efficient [34]. GOx is highly specific to glucose. Glucose

fits into GOx by a lock and fit mechanism by which the chemical reaction in the cell

takes place. Since the enzymes host the redox reaction in EBFCs, different from metal

catalysts in normal fuel cells, it is required for them to be immobilized on electrodes for

the transfer of electrons.

The challenge of EBFCs is the immobilization of the enzyme. In the early stage of

employing CNTs for the fabrication of electrodes, basically the CNTs, as electrodes, were put in the enzyme solution and this allows the electrodes to absorb the enzymes. The power output and lifetime are not ideal for this approach. But more and more improvements have been made in recent years.

Wang et al. [35] obtained a power output of $1.38\mu W/cm^2$ at an external load of 99 mV with porous silicon-carbon nanotube electrodes, whereas Katz et al. obtained a power output of $4\mu W/cm^2$ at 600mV with gold electrodes [36]. Both studies involved membrane-less operation but the study by Wang et al. involved DET by carbon nanotubes without the use of a mediator. Immobilization of the enzyme on the electrodes was performed using cyclic voltammetry by Wang et al., while Katz et al. reconstituted the enzymes chemically with the mediator molecules in order to achieve immobilization.The main problem with the above experiments was the immobilization of enzymes used which has been overcome in the present work by compression of the enzymes on the nanotube paper electrodes. Minteer et al. obtained a power output of $0.83mW/cm^2$ using ethanol and oxygen as fuels in their biofuel cell [37]. More recently, Kwon et al. developed a biscrolled yarn BFC which attained a power density of $2.18mW/cm^2$ using GOx and Bilirubin Oxidase and redox mediator [38]. Abreu et al. presented a flow through EBFC design with power output of $0.7 \pm 0.035mW$ at 0.41 V using GOx and horseradish peroxidase [39]. Another notable development was presented by Shitanda et al. using screen-printing technology to fabricate EBFC and combining five individual cells into a unit which exhibited a maximum power of 350mW at 1.55V and OCP of 2.65V [40]. These experiments showed that higher power output from EBFCs can be reached. Yet their design is quite complicated which can

bring difficulties for mass production for applications. In this dissertation, a new simple design of EBFC fabrication with techniques of mechanical compression for enzyme immobilization on CNT nanopaper electrodes was employed to prepare EBFCs in a novel sandwich patch design. The performance of this design, in comparison with conventional EBFCs, will be discussed together with preliminary experiments to understand the chemistry of EBFCs using Raman spectroscopy.

1.3 Biofuel Cell Applications

1.3.1 Implantable Biofuel Cells

Some implantable medical devices can only function with a power source such as implantable cardioverter defibrillators and cardiac pacemakers. Currently, these devices use lithium-ion batteries as their power source. However, the concern of battery leakage and poisoning of biological tissues with lithium batteries, which have insufficient biocompatibility, has never been resolved.

Since biofuel cells can generate electrical power by harvesting the chemical energies from biological matter, and with natural biocompatibility, biofuel cells, especially EBFCs, possess significant potential as a substitute for lithium batteries for power generation for implantable medical devices[41].
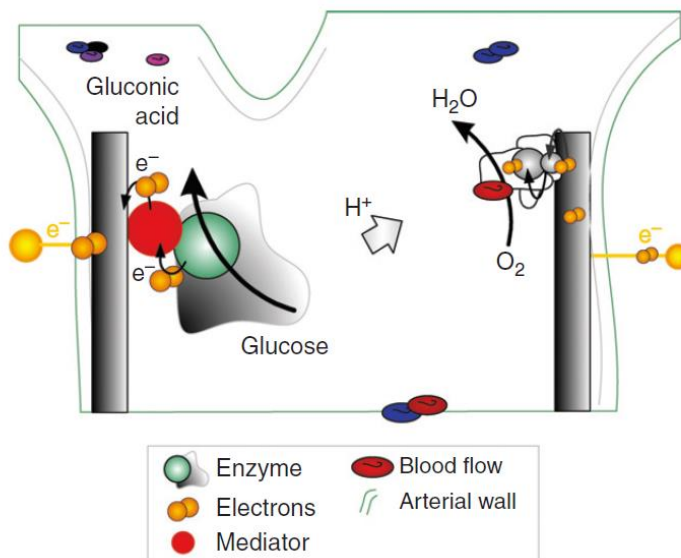
Figure 1.9 Schematic diagram of an EBFC working in blood [23]

There are many recent advancements regarding implantable EBFCs in animals. This includes an EBFC operating *in vivo* in a mouse [42]. In this research, a biofuel cell utilizing glucose dehydrogenase and laccase on the anode and cathode respectively, and PQQ mediator was used. The open-circuit voltage is 140 ± 30mV and short-circuit current is $10\pm3\mu$A with the current density of 5μA cm^{-2}. Some research has also been done on implanted biofuel cells operating in a living snail[43], cockroaches[44] and lobsters[45].
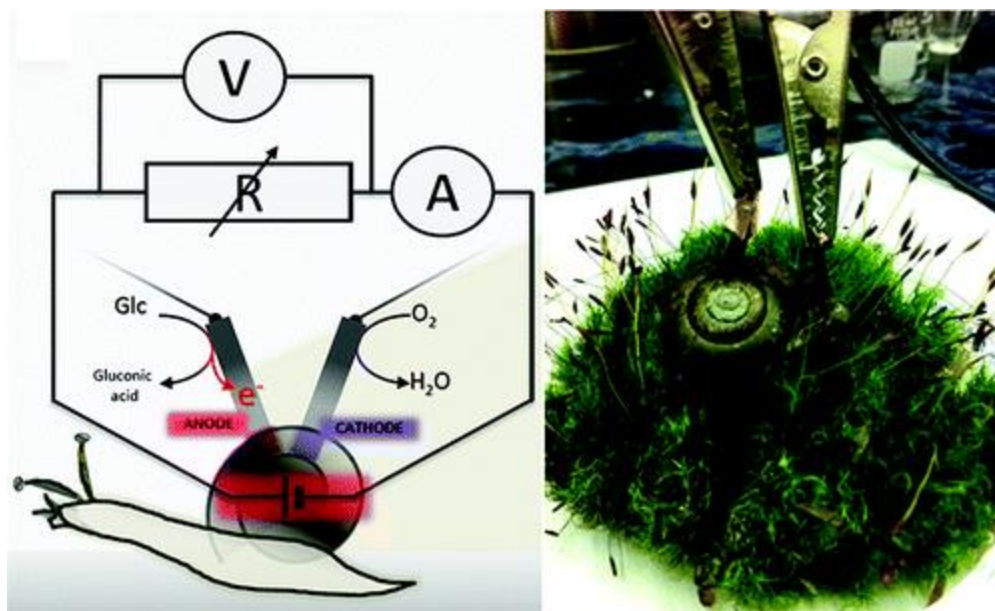
Figure 1.10 Schematic diagram and the electrical connection of a snail with implanted EBFC [43].
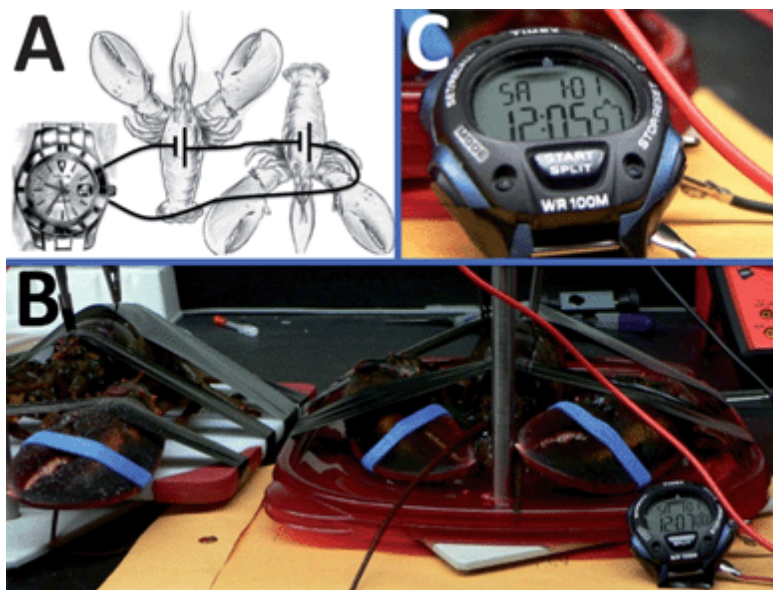
Figure 1.11 Two lobsters with implanted EBFCs wired in series to power a watch (A) The wiring scheme. (B) The photograph of the setup. (C) Close view of the operating watch [45].

1.3.1 Wearable Biofuel Cells

One application of biofuel cells that has drawn more attention than the others is the

wearable biofuel cell. Such wearable biofuel cells can be attached to human skin without the need for microneedles and can cause much less skin irritation. However, without piercing the skin, the choice of the fuel can no longer be glucose, since there is no glucose at the surface of a healthy human being. A strong candidate for this application is human sweat due to the combination of a rich variety of chemicals, sufficient source and easy to reach at the surface of human skin. As for the choice of the enzyme, lactate oxidase and lactate dehydrogenase are the perfect candidates because of the high concentration of lactate in human sweat. Wang's group has demonstrated a successful example for such an application. They developed a tattoo-based wearable biofuel cell system with the use of CNT-lactate oxidase anode and Pt cathode [46].
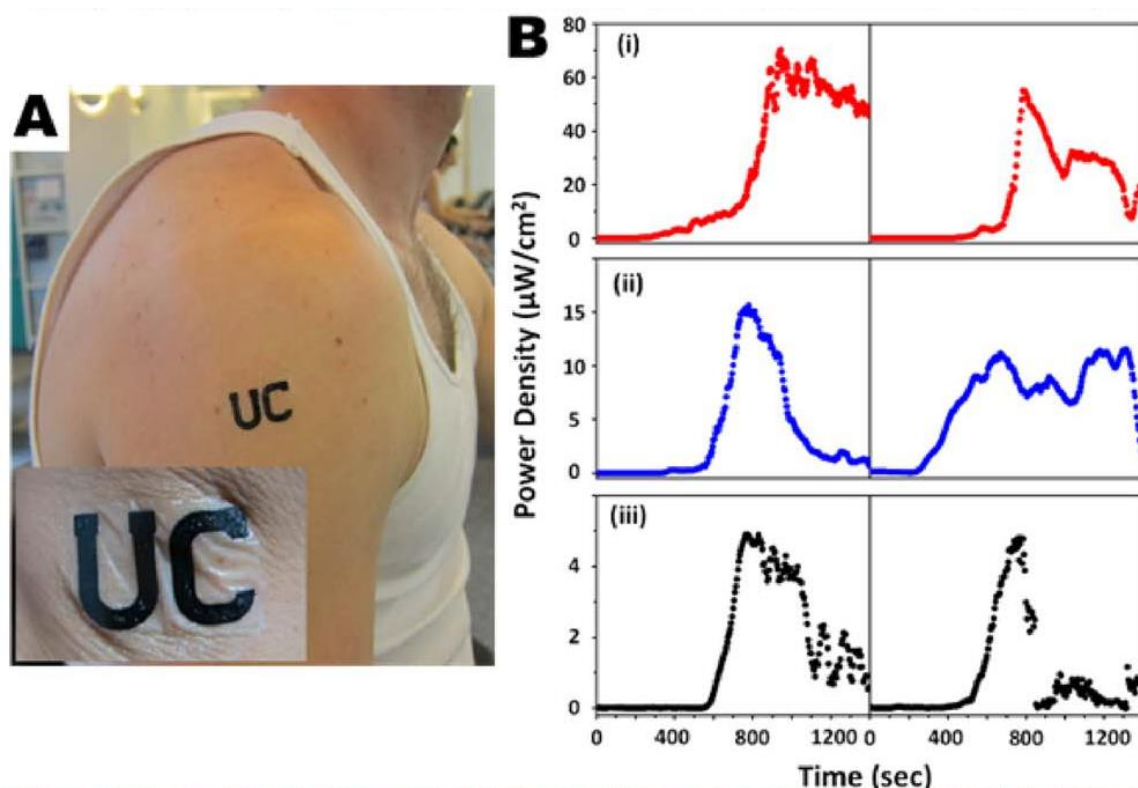
Figure 1.12 (A) Photograph of the tatto-based wearable biofuel cell (B) and the real-time power density of such an application [46].

The power generation is dependent on the fitness level of the human subjects because the lactate concentration in their sweat is different and the power density is up to 70µW/cm^2. Wang's group then further improved their design and with the integration of a DC/AC converter, they were able to boost the voltage to power low-energy consuming electrical devices, for example LEDs and wrist-watches [47].

Other researchers have adapted routes different from that of Wang's group. For example, high concentrations of different types of biofuel in a sealed EBFC unit has also been developed [48, 49]. A new EBFC design based on such a concept has been developed in this dissertation and will be discussed in Chapter 4.

1.4 Materials Characterization Techniques Used

1.4.1 Scanning Electron Microscopy (SEM)

Scanning Electron Microscopy (SEM) uses a type of electron microscope that produces images of samples by scanning the surface with a focused beam of electrons. The electrons interact with atoms in the sample to produce various signals containing information about the surface topography to produce the image. The SEM has been widely used in obtaining morphological and surface structure of samples with nanoscale resolution.
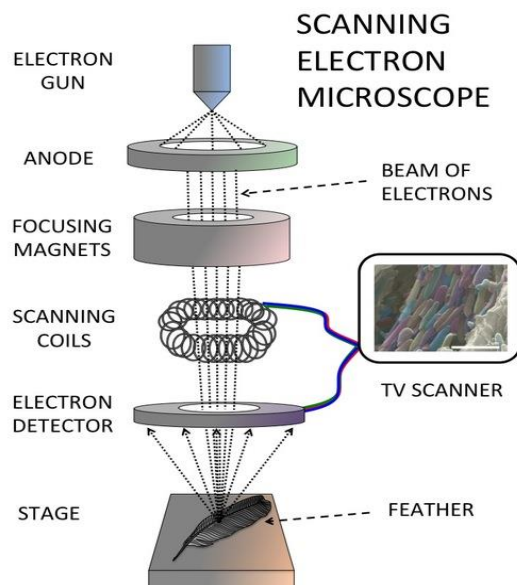
Figure 1.13 Schematic representation of a scanning electron microscope.

In this dissertation, the SEM has been used to investigate the surface morphology of CNT nanopaper sheet samples and the enzymatic electrodes before and after compression. The SEM used in this study is a field emission scanning electron microscope, VP-1530 Carl Zeiss LEO (Carl Zeiss, Peabody, MA, USA) with an Oxford EDS Detector (FESEM-EDS) located at the York Centre at the New Jersey Institute of Technology (NJIT).

Figure 1.14 FESEM-EDS in NJIT [50].
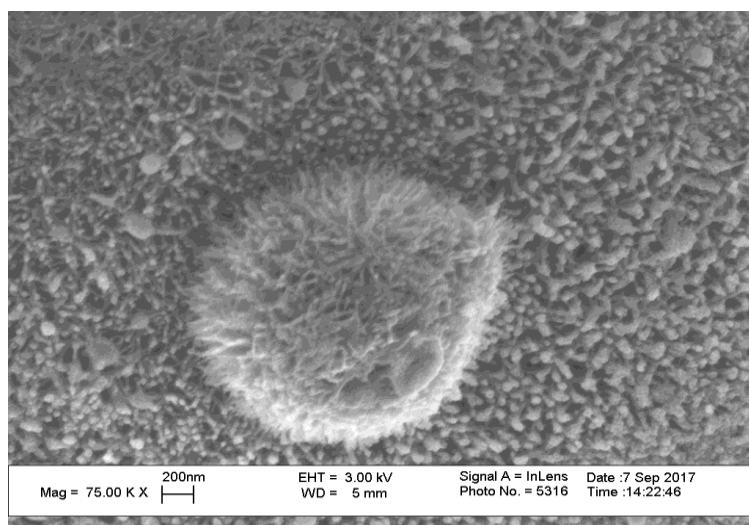
Figure 1.15 SEM image of CNTs deposited on catalyst-infiltrated aluminum powder taken by the FESEM-EDS instrument at NJIT (B. Leng and Ron Poveda – unpublished)

1.4.2 Raman Spectroscopy

Raman spectroscopy is a spectroscopic technique that utilizes inelastic scattering from a laser light source (wavelength ranging from ultra-violet to near infra-red) illuminating a sample to generate a vibrational Raman spectrum using a sensitive photon detector. Some commonly used excitation laser wavelengths are 325nm, 532nm, 633nm, and 785nm.

Compared with conventional Raman spectroscopy, Surface Enhanced Raman Spectroscopy (SERS) is much more sensitive while remaining highly specific [51, 52]. It utilizes metal nanoparticles, such as gold or silver that is deposited on the surface of a nanostructured substrate on which the sample is deposited, to provide plasmon-enhanced scattering for detection at extreme low concentrations. The detection enhancement can be as high as 10^{14} to 10^{15} allowing the detection of a single molecule [53, 54].

Figure 1.16 Thermo Fisher DXR Raman Microscope used for Raman scattering studies in this dissertation. [55]

A general electrochemical redox reaction of the glucose based EBFC has been described in Section 1.2. The Flavin Adenine Dinucleotide (FAD) cofactor, a very common enzyme in proteins, plays an important role in such reactions [24, 30-32]. Therefore, it is worth taking a closer look into the mechanism of the redox reaction by SERS. The SERS signal of GOx is mainly due to the FAD in the redox center of the enzyme protein[56]. Further details are given in the figure caption of Figure 1.17 and the assignments of Raman vibration modes of GOx are provided in Table 1.3.
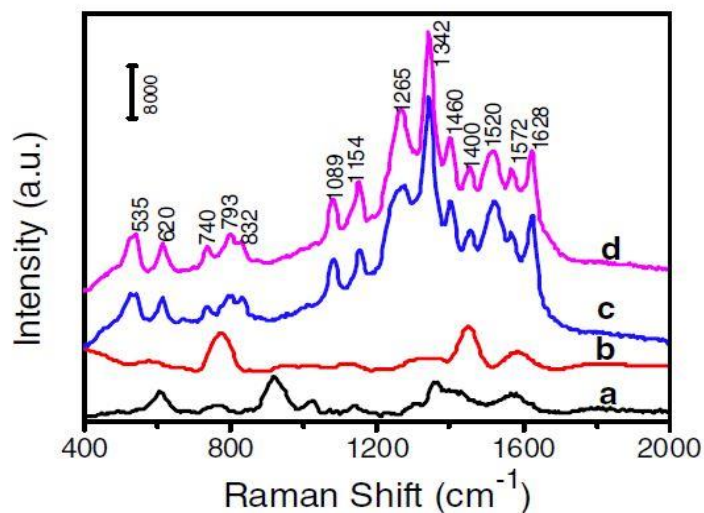
Figure 1.17 SERS for GOx detection [53].

In Figure 1.17 the different line indicating as follows SERS of silver nanoparticle assembled film (a); SERS of PDDA-Ag film assembled film (b); the GOx-functionalized SERS chips (c); and the GOx-functionalized SERS chip dipped in glucose in the blood serum (d). PDDA- poly(dimethyl diallyl) ammonium chloride is a linker molecule used to stabilize the silver nanoparticles on the glass substrate.

Table 1.3 Assignments of Raman Vibrations Modes of GOx [57]

Wave number (cm^{-1})	Vibrational assignments
1628	ν C–C–C
1572	ν C=N
1520	ν C=N
1460	ν C=C + δ CH$_3$
1400	ν N–C=O + ν C=C + ν C–C
1342	ν C–C=N + ν C=C + δ CH$_3$
1265	δ CH$_3$ + δ N–H
1154	ν C–C + ν C–CH$_3$ + ν C–N + δCH$_3$
1089	β C–H + ν C–N
832	γ C–H
793	β C–C–C
740	ω NH$_2$ + γ C–C–C
620	β C–C–C
535	γ C–C–C

Table 1.3 lists all the assignments of SERS signal for GOx. It can be utilized as a guide to recognize the presence of GOx in the samples.

1.5 Organization of this Dissertation

In the first chapter of this dissertation, an introduction to the concepts and mechanism of different types of biofuel cells is addressed. Developing a new EBFC with better performance and improved design is needed. Characterization techniques such as field-emission scanning electron microscopy to investigate the surface morphology and Surface Enhanced Raman Spectroscopy to monitor the electrochemical reaction mechanism is introduced.

Chapter 2 presents an overview of the types of CNTs including single wall carbon nanotubes (SWCNTs) and multiwall carbon nanotubes (MWCNTs) and the corresponding synthesis methods.

Chapter 3 details the proposed bio-electrode research involved in this study, including how CNT nanopapers, which serve as the base material for the electrodes, are prepared for the fabrication of EBFCs and the design and test of different types of bio-electrodes used in this dissertation.

Chapter 4 details the newly proposed concept of sandwich form EBFC patch research of this study. The proposed EBFC patch design is based on the bio-electrode developed in Chapter 3. The performance of power output and lifetime of such EBFC patches is addressed in this Chapter and compared with the results from conventional BFCs using similar electrodes. Results of the study on BFCs with laccase at the cathode replaced by Pt will be discussed.

Chapter 5 presents a conlusion of the research study conducted in this dissertation by summarizing the results and providing recommendations of directions to further improve the performance of the patch EBFC design.

Appendices A and B present preliminary research involving *in-situ* Raman spectroscopy of GOx in the EBFC patch anode under electrochemical load to investigate the electrochemical reactions that are taking place with the goal of eventually optimizing the electrode design. Appendix C discusses a 24-hr monitoring system that has been developed to monitor EBFC performance and Appendix D presents preliminary results on the use of a metal free polymeric nitrogen oxidation reduction reaction catalyst that can potentially replace laccase.

CHAPTER 2

CARBON NANOTUBES

2.1 Fundamentals of Carbon Nanotubes

Carbon is a material that has been extensively studied for a very long time. There are a number of allotropes of carbon that have been discovered years ago, such as graphite, diamond, and the fullerenes, and more recently, carbon nanotubes and graphene. Carbon nanotube (CNT) is one type of allotrope of carbon that has a cylindrical nanostructure. CNTs can be categorized into two classes, multi-walled carbon nanotubes (MWCNTs) and single-walled carbon nanotubes (SWCNTs). The first observation of MWCNTs was made by Iijima in 1991 while applying direct current arc at graphite electrodes [58]. Two years later, SWCNTs were discovered by Iijima and Ichihashi in 1993 [59].

The SWCNTs can be thought of as a layer of graphene nanoribbon that is bent and then rolled up into a hollow cylindrical form.

graphene sheet   SWNT
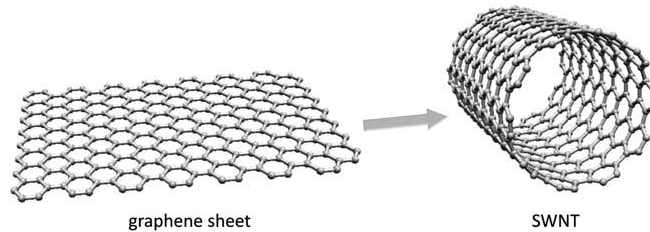
Figure 2.1 Wrapping of graphene nanoribbon into SWCNT [60].

Depending on how the graphene nanoribbon is wrapped, the properties such as mechanical, electrical, optical etc. will change[61]. A chiral vector $\vec{C}$, as a result of a pair of integers (n, m) of the graphene honeycomb vectors $\vec{\alpha_1}$ and $\vec{\alpha_2}$, can show how

the graphene is wrapped. Generally, there are three types of constructions of SWCNTs according to the integers (n, m). When m=0, which is (n, 0), this kind of structure is called "zigzag". When n=m, which is (n, n), this kind of structure is called "armchair". The third type of structure is when n>m>0, and it is called as "chiral" (Figure 2.2). The diameter of SWCNTs is around a few nanometers.
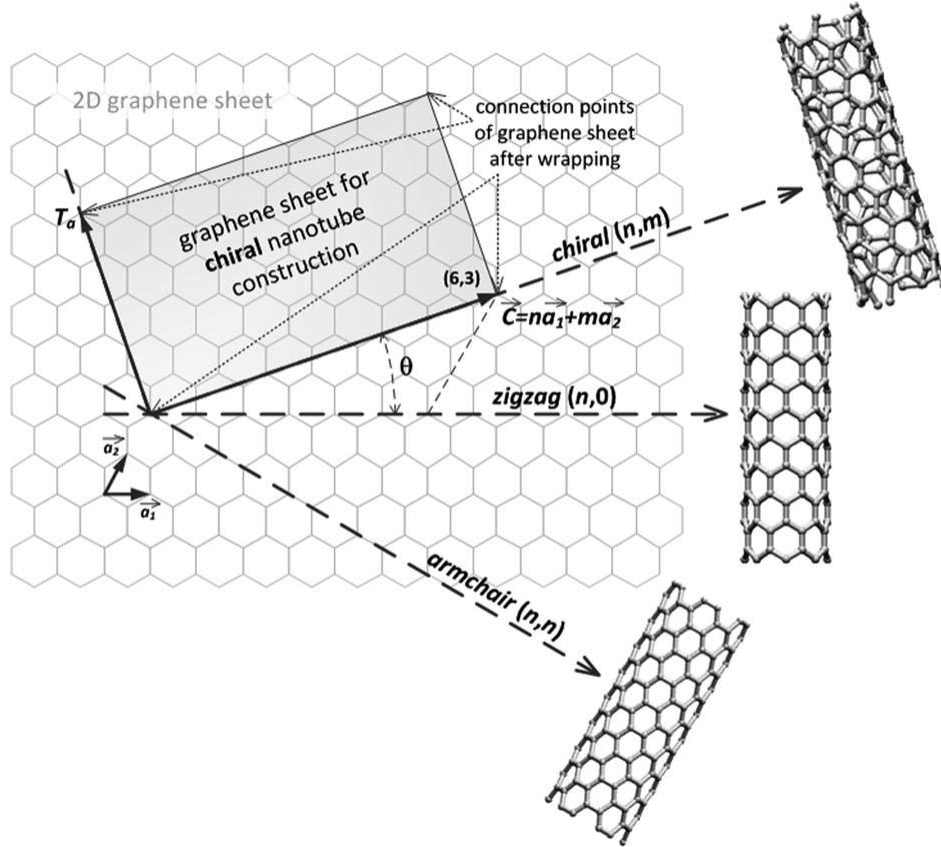
Figure 2.2 Schematic of the construction of SWCNT structures [60].

The structure of MWCNTs consists of multiple concentric tubes of rolled up graphene which has a diameter ranging from several nanometers to tens of nanometers. Depending on the construction of MWCNTs, there are two models that can describe their structures, the Russian doll model and Parchment model. The structure of Russian

Doll model consists of multiple sheets of graphite that are arranged very similar to the Russian dolls which have multiple cylindrical graphite sheets wrapped one on top of the other from inside out. The Russian Doll structure is observed more commonly. Each individual shell of rolled graphite sheet can be described as a SWCNT, which can be metallic or semiconducting. Because of statistical probability and restrictions on the relative diameters of the individual tubes, one of the shells, and thus the whole MWCNT, is usually a zero-gap metal [62].

As for the Parchment model, the structure is one single sheet of graphite being rolled around itself, like a scroll of parchment or a toilet roll. The distance between layers of graphite sheets in MWCNTs is close to the distance between graphene layers in graphite, approximately 3.4 Å.
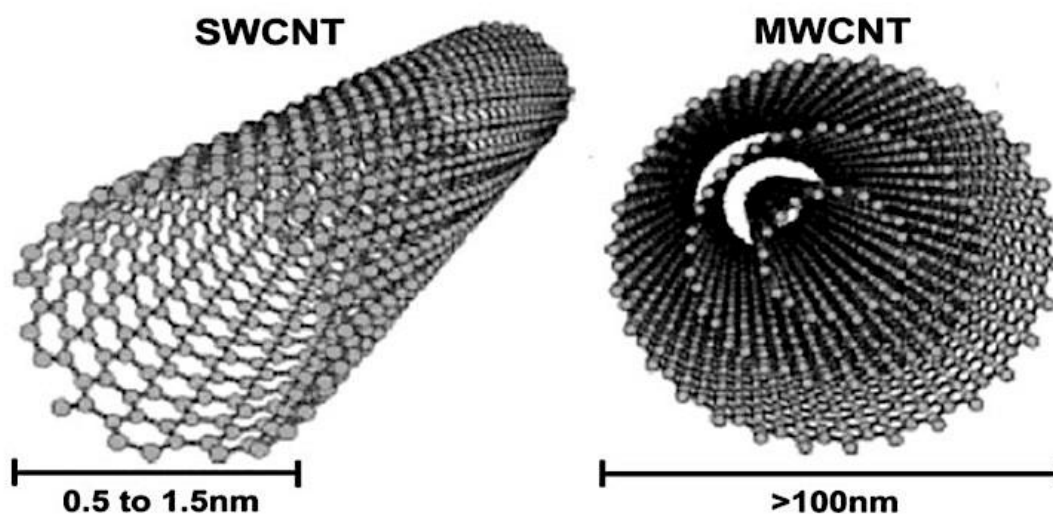
Figure 2.3 Schematic representation of single walled carbon nanotube (SWCNT) and multi walled carbon nanotube (MWCNT) [63].

2.2 Synthesis of Carbon Nanotubes

2.2.1 Arc Discharge

The first synthesis method of CNTs was Arc discharge. Originally, it was introduced to produce C_{60} by Krätschmer et al. in 1990 [64]. It was then used by Iijima et al. [58] to discover MWCNTs. The arc discharge synthesis of MWNTs usually utilizes a hot plasma between two graphite electrodes in a helium filled chamber. The chamber is maintained at sub-atmospheric pressure and at high temperatures (over 1700C), as the carbon atoms are evaporated while a high DC current passes through the electrodes. The CNTs are then deposited on the cathode.
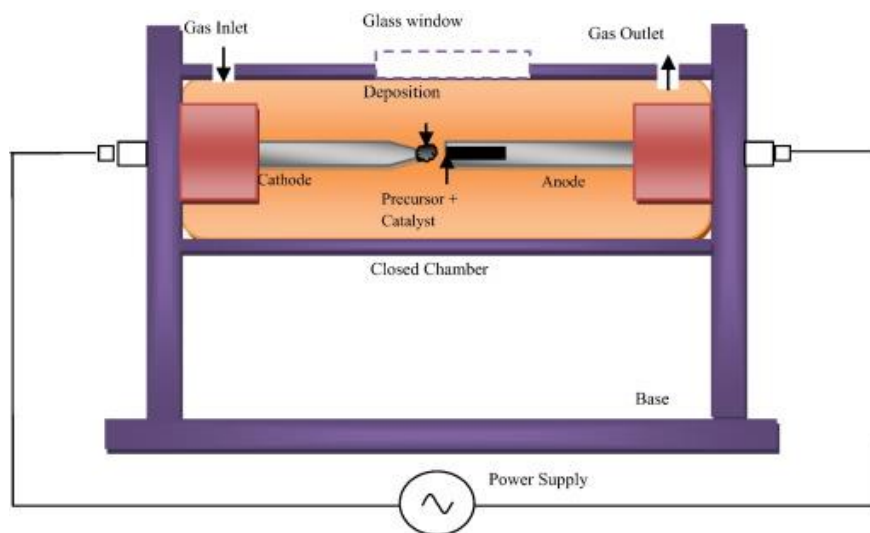
Figure 2.4 Schematic diagram of the arc discharge setup [65].

It has been reported that, with different gases filled in the chamber, the quantity and purity of MWCNTs are different [66-68]. The yields of MWCNTs can be increased with increase in pressure [69].

Using arc discharge method, without any catalyst, results in the deposition of MWCNTs. But with the use of catalyst or catalyst precursors, such as Ni, Co or Pt,

SWCNTs can be formed after the process. It was first demonstrated by Bethune et al. in 1993 [70].

2.2.2 Laser Ablation

The principle of laser ablation is similar to arc discharge method; the difference is that instead of a hot plasma, a YAG or CO_2 laser provides the energy for the process. Usually, a graphite pellet containing Ni or Co as the catalyst is used during the process. This method can yield SWCNTs with higher quality and purity compared to arc discharge method. It was first demonstrated by Guo et al. in 1995 [71].
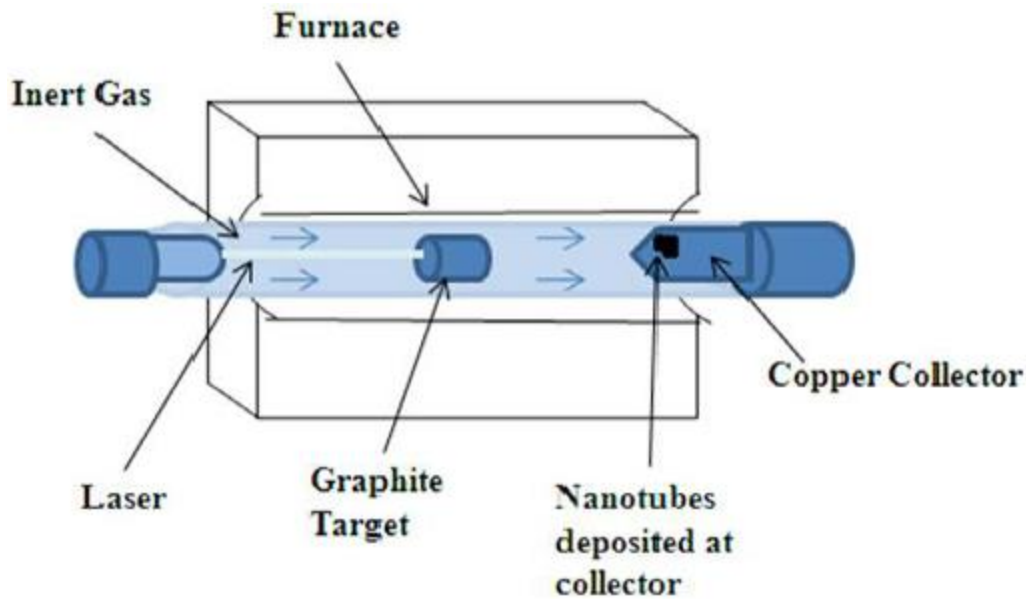
Figure 2.5 Schematic diagram of laser ablation setup [72].

2.2.3 Chemical Vapor Deposition (CVD)

Currently, the standard method for the production of CNTs is Chemical Vapor Deposition. There are numerous subclasses of CVD, such as Plasma Enhanced Chemical Vapor Deposition (PECVD), Microwave plasma (MPECVD), radiofrequency CVD (RF-CVD), etc. The CVD method is considered as the most economical and successful

method for the production of CNTs because it can not only produce considerably good quality of CNTs but it can also produce good quantities at the same time. It does not need high temperature like the other two methods to evaporate solid carbon source. The first report of production of CNTs by CVD method was made by Endo et al. in 1993 [73]. A carbon gas source and precursor with carrier inert gas are passed through a quartz tube which is heated by a furnace. A catalyst (such as cobalt, nickel, iron etc.) covered substrate is placed within the active area of the quartz tube and heated at temperatures ranging from 600℃ to 1200℃ during the CVD process. The carbon source for CNT growth is typically hydrocarbons such as methane, ethane, acetylene, xylene, etc. [74-77].
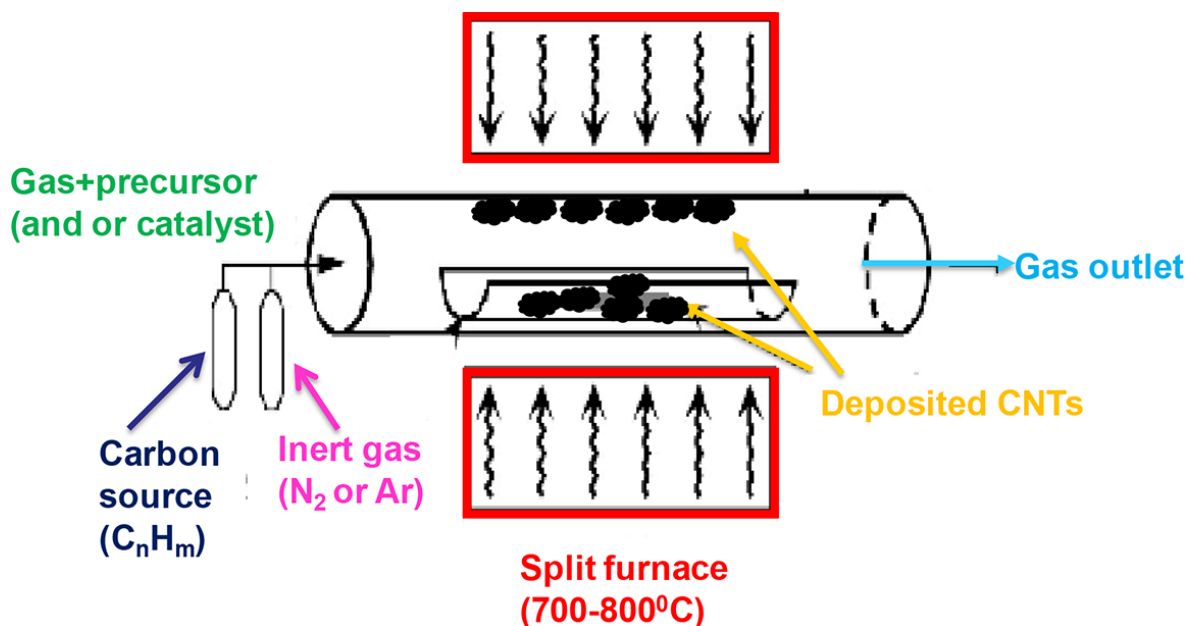
Figure 2.6 Schematic diagram of Chemical Vapor Deposition setup [78].

In CVD process, different catalysts can affect the growth of CNTs significantly. Feng et al. used acetone as a carbon source, Ferrocene($C_{10}H_{10}Fe$) as a source of Fe catalyst and thiophene as promoter to synthesize high quality DWNT (Double Wall

carbon nanotube) thin-films in a one-step CCVD (Catalytic CVD) reaction process in an argon flow[79]. Li studied the synthesis of well aligned MWNTs on a large area of Ni deposited SiO_2/Si substrates via the pyrolysis of C_2H_2 using the thermal CVD technique at 900^oC. Li found that NH_3 pretreatment was very crucial to control the surface morphology of catalytic metals and thus to achieve the vertical alignment of CNTs. With a higher density of Ni particles, better alignment of the CNTs can be obtained due to a steric hindrance effect between neighboring CNTs. The degree of crystallization of the CNTs increased with increasing NH_3 pretreatment time. Energy dispersive X-ray analysis revealed that CNTs grew by a tip growth mechanism [80]. Liu and colleagues recently published a comprehensive review on direct CVD growth of aligned, ultralong SWNTs on substrate surfaces, which are attractive building blocks for nano-electronics. They discussed the key technical points, mechanisms, advantages, and limitations of this method [81]. Flahaut et al. reported the influence of catalyst preparation conditions for the synthesis of CNTs by CCVD. In their work, the catalysts were prepared by the combustion route using either urea or citric acid as the fuel. They found that the milder combustion conditions obtained in the case of citric acid can either limit the formation of carbon nanofibers or increase the selectivity of the CCVD synthesis towards CNTs with fewer walls, depending on the catalyst composition [82]. Xiang et al. prepared CNTs via CCVD of acetylene on a series of catalysts derived from Co/Fe/Al layered double hydroxides (LDHs). They observed that the content of Co in the precursors had a distinct effect on the growth of CNTs. Increasing Co content enhanced the carbon yield due to good dispersion of a large number of active Co species. Higher Co content led to the formation of CNTs with smaller diameters and less

33

structural disorder [83]. Lyu et al. produced high-quality and high-purity DWNTs by catalytic decomposition of benzene as an ideal carbon source and Fe–Mo/Al$_2$O$_3$ as a catalyst at 900°C. They obtained DWNT bundles, free of amorphous carbon covering on the surface, and of a low defect level in the atomic carbon structure [84]. Zhang et al. prepared MWNTs with diameters of 40–60 nm by the catalytic decomposition of methane at 680°C for 120 minutes, using nickel oxide–silica binary aerogels as the catalyst [85].

2.3 Use of Carbon Nanotubes in EBFCs

Shortly after the discovery of CNTs, it did not take long time before researchers started to investigate the possibility of combining the CNTs with EBFCs. This topic has been studied intensively in the recent decade. The research on the use of CNTs in EBFCs is mostly concentrated on the immobilization of the enzymes on CNTs for better electron transfer rate to achieve higher power output and longer lifetime.

Some techniques that are commonly used in combining the CNTs with EBFCs are drop casting [86], covalent binding of CNTs [87], direct growth of CNT forests on the electrode [86], deposition of MWCNT film by microcontact printing technique [88], and co-deposition of CNT-doped polymers etc. [89].

The technique for the immobilization of enzyme on CNTs, used in this dissertation, will be discussed in detail in the next Chapter.

Figure 2.7 shows the SEM images of CNTs prepared by different techniques.
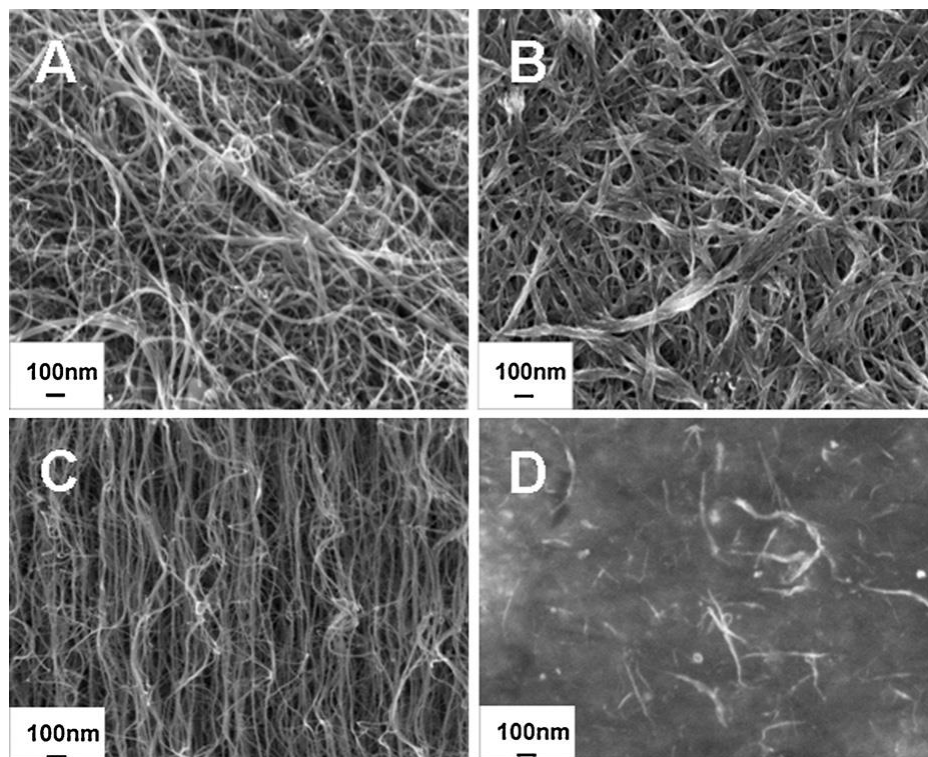
Figure 2.7 Representative SEM micrographs of (A) MWCNT and (B) SWCNT deposits, (C) aligned CNT forests, and (D) CNT doped polymers [90].

The CNTs used for the fabrication of bio-electrodes, in this dissertation, was purchased from nano-lab.com. These CNTs are multiwall carbon nanotubes that were produced by Chemical Vapor Deposition (CVD) to strict length and diameter specifications, and are purified to >95% as measured by TGA.

Figures 2.8 and 2.9 show the characterization results from Nano-lab Inc. for CNTs (Catalog No.PD15L520) that is used in this dissertation.
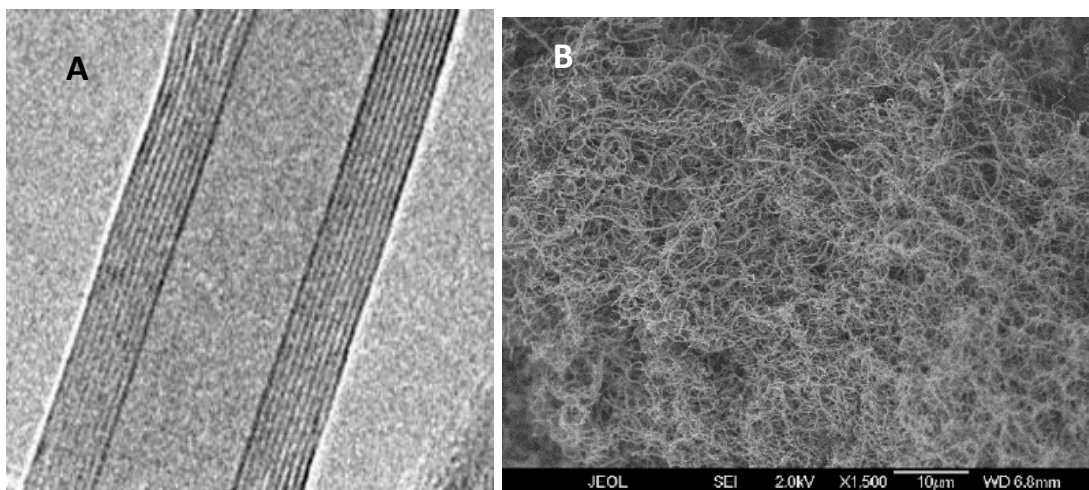
Figure 2.8 (A) Multi wall Carbon nanotube TEM image, PD15L520 10- walls, diameter 12nm [91], (B) Multiwall Carbon nanotube SEM image, PD15L520 [92].
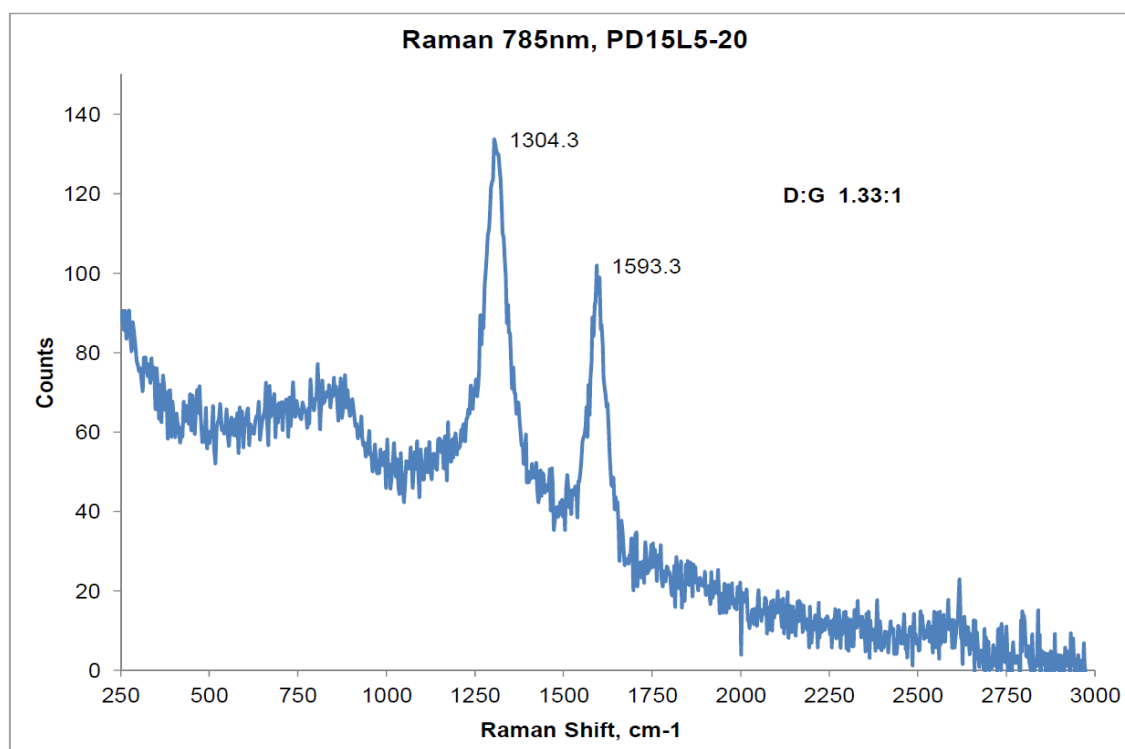
Figure 2.9 Multi wall Carbon nanotube Raman data PD15L520 D:G ratio 1.33:1 [93].

CHAPTER 3

DESIGN AND TEST OF ENZYMATIC BIOFUEL CELL ELECTRODES

3.1 Challenges

Currently, enzymatic biofuel cells are facing the challenges of lower than desirable performance, such as short life time, low power density and complex fabrication and assembly process etc. In order to improve the electrochemical performance of the EBFCs, strategies can be taken regarding the open circuit potentials, current density and power densities because these factors are essential in the evaluation of EBFCs performance. For the improvement of open circuit potential, with MET based system, one needs to find a mediator with potentials closer to the potentials of redox enzyme. Some mediators, for example osmium complexes [94, 95] and 2,2′-azinobis (3-ethylbenzthiazoline)-6-sulfonic acid [96], have been reported as feasible choice to be incorporated with glucose biofuel cell fabrication. However, with the introduction of mediator, it can bring more issues. Not only the mediator lowers the open-circuit potential of the EBFC, but also the procedure of the immobilization of a mediator on the electrode is often complicated. The stability of the mediator also affects the performance of EBFC over time [34]. Therefore, a DET based system, if possible, would be a better solution to improve the open circuit potentials of EBFCs.

As for the improvement of current density and power density, methods can be adapted for high rate of catalytic activity of the enzymes and faster electron transfer rate between enzymes and electrodes. Enzyme engineering can be a good strategy. Technologies based on synthetic biology can be utilized to obtain smaller enzymes in

volume, but with higher catalytic activity or construct more efficient pathways within the enzyme molecule for direct electron transfer [97-99]. Another strategy is to utilize high surface area electrode materials such as MWCNTs. As discussed in Chapter 2, MWCNTs are excellent materials for the fabrication of EBFC electrodes.

To improve the life time of EBFCs, immobilization and stabilization of enzymes at electrodes is crucial. In the early studies, electrode was simply incubated in an enzyme solution [100]. This method is not an optimal immobilization technique due to the fact that it promptly dissolves the enzyme into the electrolyte. Some improvements have been made with covalent bonding and crosslinking of enzyme with polymer hydrogel [101] and gold electrode surfaces [102]. These methods have indeed improved the stability of enzyme at electrodes, but they have also decreased the activity of enzymes [16]. Sandwich and encapsulation techniques were designed by Akers et al. [103], Koltzbach et al. [104], and Moore et al. [105], to immobilize an enzyme at the surface of an electrode. In 2011, Zebda et al. proposed an interesting and efficient method by mechanically compressing the MWCNTs with enzyme directly as an electrode which delivered not only high power density and high open circuit voltage but also maintained its stability for 1 month [106]. All these approaches have paved the way for further improvements in the performance of EBFCs.

With the scientific challenges addressed, this dissertation first presents a new principle of bio-electrode design with several different configurations in this chapter. Then a detailed discussion regarding the EBFC unit design is presented in the next chapter.

3.2 Design and Fabrication of Electrodes

In order to address both power density and lifetime related issues, this dissertation presents a new principle of bio-electrode design combining the use of functionalized MWCNTs and mechanical compression. Functionalized MWCNT is ideal for bio-electrode fabrication because it has high surface area to entrap the enzyme and allow DET between active redox site and electrode surface. Mechanical compression acting as the immobilization technique of enzyme can not only improve the DET mechanism but also the entrapment of enzyme, which leads to a better stability of the bio-electrode.

The materials used for the fabrication of the electrodes are as follows. Carbon paper (E-TEK,Inc) was used as received. The wetness was 60%. Carbon nanotubes (MWNTs) (Carbon Solutions, Inc.) were used as received. Ethanol was purchased from Fisher Scientific Inc. Glucose-oxidase (GOx, 200U/mg, Aspergillus niger, Sigma), Laccase (Lac, 7.59 U/mg, Agaricus Bisporous, Fulka), Sodium Dodecyl sulfate (SDS, Sigma), and d-glucose (Sigma) were used as received. Nafion® (Aldrich) was used as received.

The CNT papers were prepared by vacuum filtration of aqueous suspensions of carbon nanotubes. MWCNTs were mixed with sodium dodecyl sulfate and phosphate buffer of pH 7.4. The mixture is sonicated to obtain a homogenous mixture formation at conditions of 75% amplitude, for 30 minutes at a pulse of 30 seconds with 10 seconds in interval. The CNT suspension is then filtered by vacuum filtration process for the nanopaper formation.
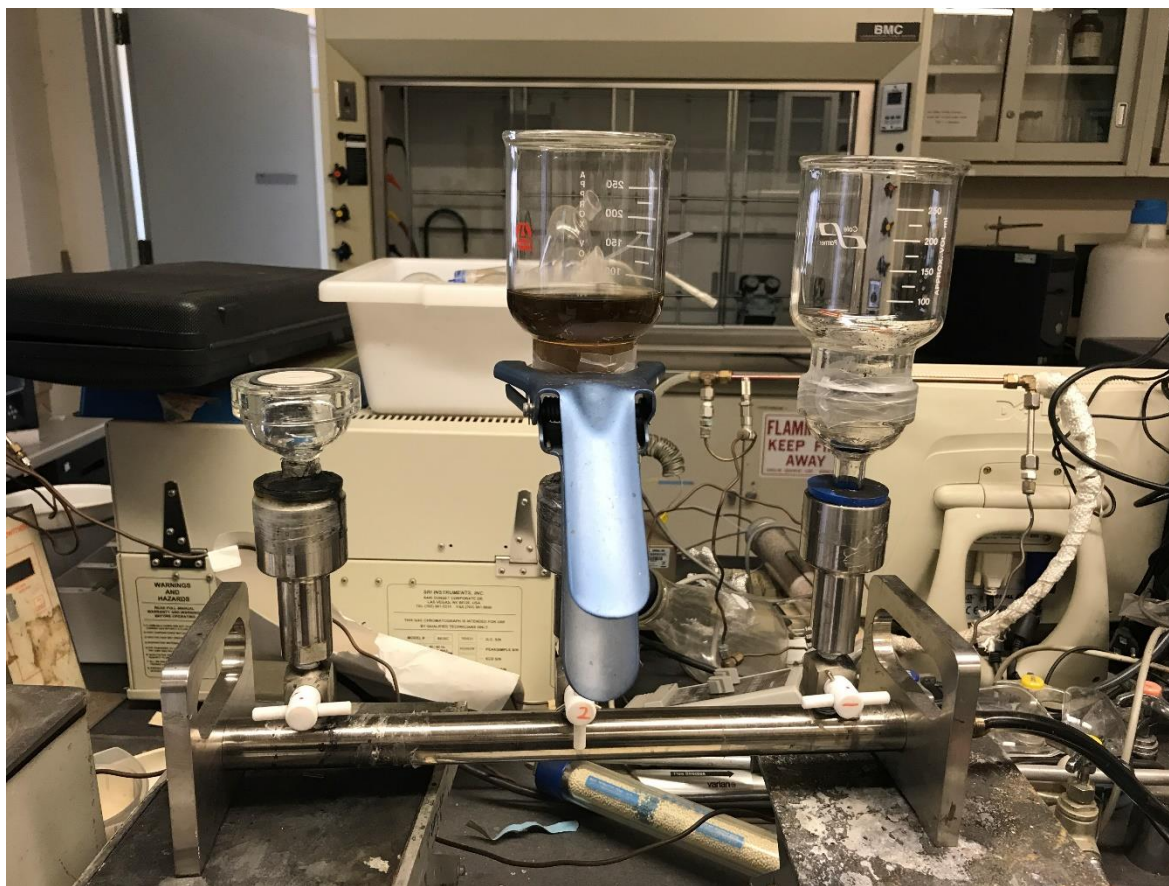
Figure 3.1 The vacuum filtration system used to produce CNTs nanopaper.

The filter papers used are of 10μm pore size. Filter papers are dipped in 10ml ethanol for 10 min before the vacuum filtration. The nanopapers were washed with 100 ml DI water for couple of hours to remove the particles.
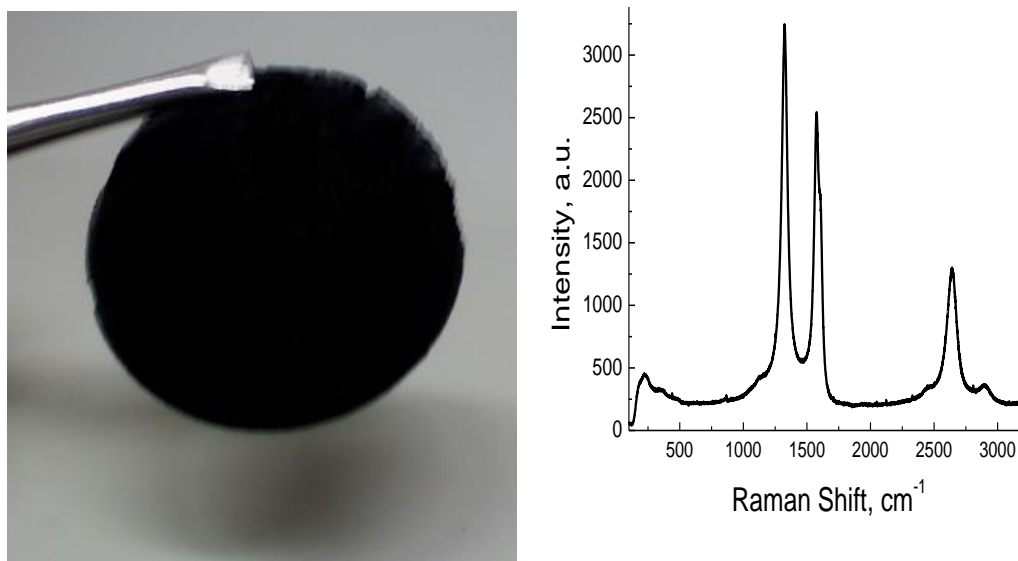
Figure 3.2 Carbon nanotube paper made with MWCNTs (left) and Ramen spectrum of the CNT paper.

After the CNT paper has been prepared, few drops of Nafion® solution (Sigma Aldrich) were dropped on the CNT paper and then dried in a vacuum oven at 90°C for 10 minutes. Thus, a layer of Nafion is formed on the nanopaper.
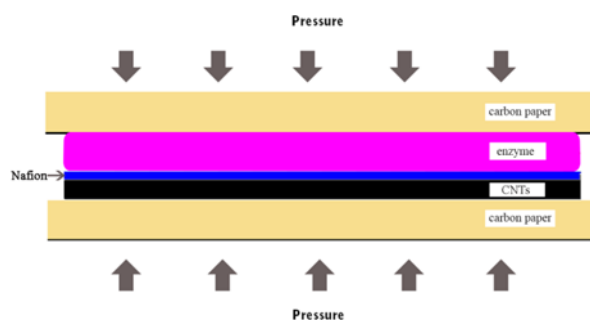
Figure 3.3 Enzyme immobilization by compression in a Carver press [107].

The CNT paper, modified with Nafion, was taken and fabricated with mechanical compression of glucose oxidase (GOx) using mechanical compression at a load of 10 metric tons. Carbon papers were used to protect the nanopapers from the pressure. Thus, a sandwich of carbon nanotubes, Nafion® and GOx were formed which is used as the

anode.

Figure 3.4 The Carver press used for the mechanical compression process.

Cathode was fabricated by the same method and laccase was used as the cathode catalyst.

3.3 Performance of Electrodes

To test the performance of the electrodes, a working EBFC setup is needed. Figure 3.3 shows a schematic of the EBFC setup. The prepared anode and cathode were assembled in a beaker with d-glucose (Sigma Aldrich) including phosphate buffer solution (PBS, pH 7.4, Fisher Scientific Inc.) as electrolyte at room temperature (20-23°C). The distance between cathode and anode was set as 5mm. The electronic circuitry is

assembled with variable resistor (RS-201 Resistance Substituter, IET Labs, Inc.), voltmeter and multimeter to measure voltage and current of EBFC.
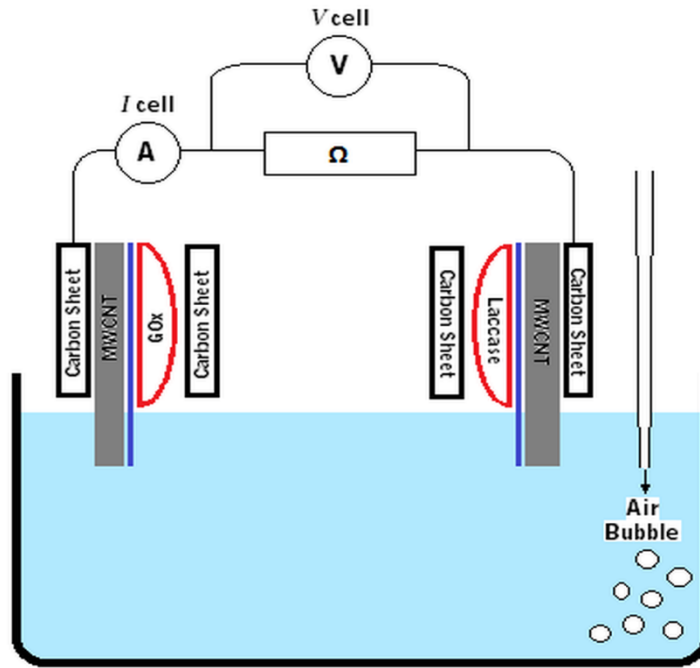
Figure 3.5 Schematic for Conventional Biofuel Cells [107].

According to the previous study reported by Qin Zhong in our laboratory[107], the optimum enzyme amount for this approach is around 40mg for both GOx and laccase of area of ~ 1cm^2 used to fabricate the bio-electrodes.

Tests of several samples fabricated according to the protocol shows similar results for the range of 30-50mg of GOx and Laccase.

The lifetime of such electrodes was tested (Figure 3.6). It can be observed that the peak performance was reached after few days. Different from the EBFC patch design, which will be discussed in the next chapter, there is a delay in peak performance due to the use of carbon paper protection on the electrode surface. This is to prevent the enzyme from dissolving into PBS, but consequently delays the maximum power output.
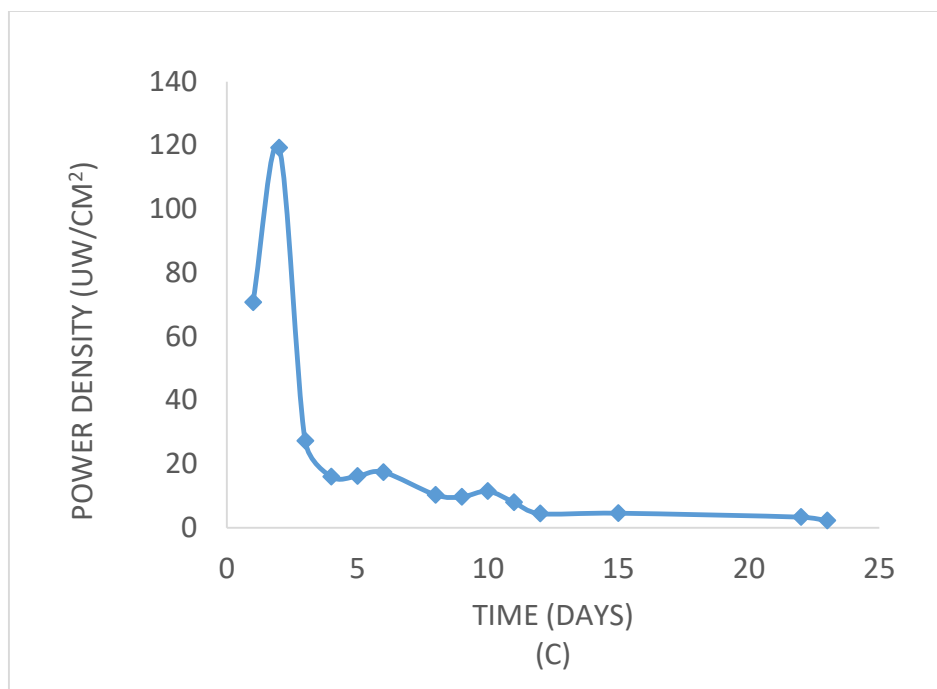
Figure 3.6 Lifetime performance of conventional EBFC test setup (average of 3 runs).

The lifetime test result in Figure 3.6 was chosen from three independent experiments but followed the same protocol. An average of over-three-weeks of data was chosen in the plot; the actual running time can be longer but is not considered for power density lower than 2 μW/cm^2. Tests of the samples after one month still show some current generation indicating that power can still be generated, even though it is limited.

These preliminary results show that the immobilization technique with mechanical compression is feasible and a detailed investigation is required.

CHAPTER 4

SANDWICH ENZYMATIC BIOFUEL CELL: DESIGN AND TEST

4.1 Cell design and Fabrication

With the feasibility of electrode design having been examined, a more realistic question is how to put it into use in real life applications. Conventional EBFC setup is by no means a sound solution to this question; all current design only exists in research labs. In this chapter, a novel simple design of EBFC patch unit with the potential for mass production and commercialization is presented.
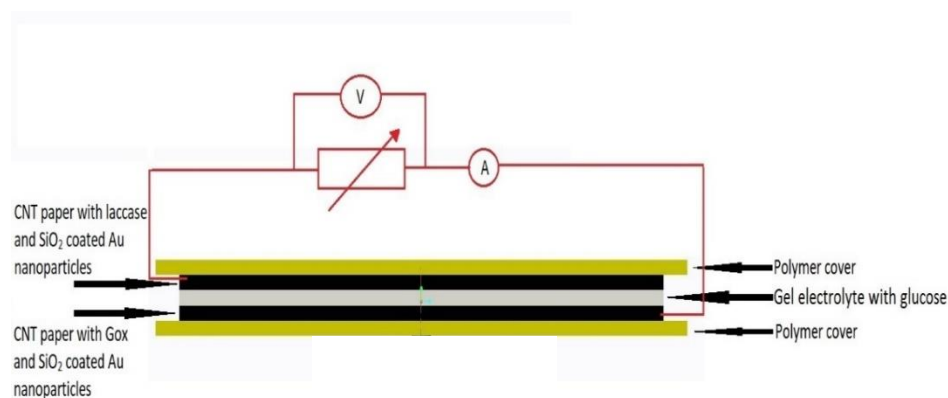
Figure 4.1 Schematic of Enzymatic Biofuel Cell Patch design.

As shown in Figure 4.1, the principal idea of this EBFC patch is that one layer of gel electrolyte containing gulcose be placed in between bio-anode and bio-cathode, then wrapped around with polymer cover with conductive wires for external circuit connection.

To fabricate such an EBFC patch, the bio-anode and bio-cathode as well as the gel electrolyte needs to be prepared before the final assmbly. The preparation protcol is as follows.

The materials used for the fabrication of the EBFC patch: Carbon paper (E-TEK, Inc) was used as received. The wetness was 60%. Carbon nanotubes (MWCNTs) (NanoLab, Inc.) were used as received. Ethanol and 0.1M phosphate buffer saline (pH 7) and phosphate buffer solution (PBS, pH 7.4) were purchased from Fisher Scientific Inc. Glucose-oxidase (GOx, 200U/mg, Aspergillus niger, Sigma), Laccase (Lac, 7.59 U/mg, Agaricus Bisporous, Fulka), Sodium Dodecyl sulfate (SDS, Sigma), and d-glucose (Sigma) were used as received. Agar (Gracilaria, TIC Gums) was used as received. Nafion® (Aldrich) was used as received. Platinum on graphitized carbon (10 wt. % loading) was purchased from Sigma Aldrich and used as received.

- MWCNTs are mixed with sodium dodecyl sulfate (SDS) and phosphate buffer of pH 7.4.

- The mixture is sonicated at conditions of 75% amplitude, for 30 minutes at a pulse of 30 seconds with 10 seconds of interval to form aqueous suspensions of CNTs.

- The aqueous suspensions of CNTs are filtered by vacuum filtration process. The filter papers used are of 10μm pore size. Filter papers are dipped in 10ml ethanol for 10 min before the vacuum filtration process. The nanopapers were washed with 100 ml DI water for couple of days to remove the residue particles.

- A free standing CNT nanopaper is peeled off from the membrane filter.

- Several drops of Nafion® were dropped on the prepared CNT nanopaper and then dried in vacuum oven at 90°C for 10 minutes. Thus, a layer of Nafion® is formed on the nanopaper.

- Designated amount of GOx powder are evenly dropped onto Nafion® modified CNT nanopaper, followed by subjecting to a hydraulic press at a load of 10 metric tons. Carbon papers are placed over the CNT nanopaper for protection purposes.

Cathode has two designs. Type 1 cathode is still a bio-electrode which was fabricated following the method as described above and instead of GOx, Laccase was

used as the enzyme for the cathode catalyst. The fabrication protocol of Type 2 cathode

is as follows.

- MWCNTs are mixed with sodium dodecyl sulfate (SDS), platinum on graphitized carbon (10 wt. % loading) and phosphate buffer of pH 7.4.

- The mixture is sonicated at conditions of 85% amplitude, for 45 minutes at a pulse of 30 seconds with 10 seconds of interval to form aqueous suspensions of CNTs and Pt.

- The suspension is then filtered by vacuum filtration process. The membrane filter used are of 10μm pore size. Filter papers are dipped in 10ml ethanol for 10 min before the vacuum filtration process. The nanopapers were washed with100 ml DI water for couple of days to remove the residue particles.

- Finally, a free standing CNT-Pt nanopaper is peeled off from the membrane filter and used as a cathode.

For the preparation of agar gel electrolyte, PBS with glucose was heated to a

temperature of 90°C and kept for 20 minutes. The mixture was mixed thoroughly and

then cooled in a container where a homogenous gel was formed.
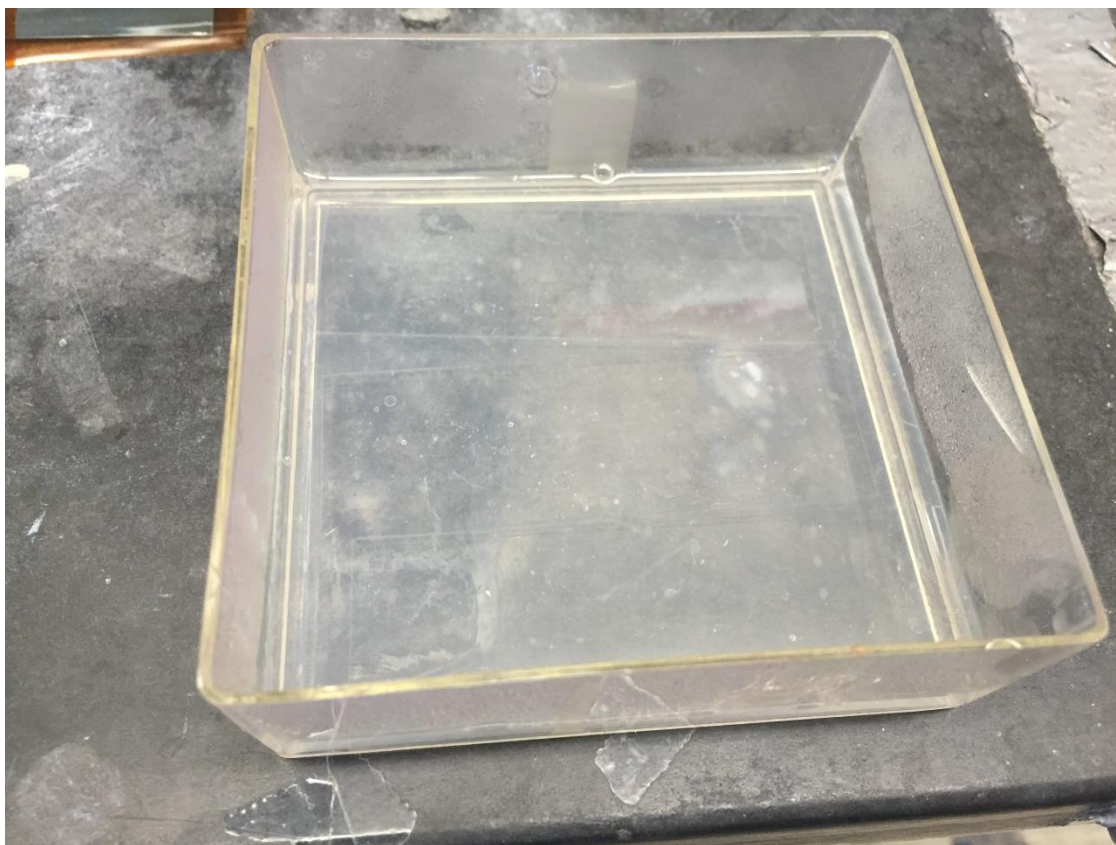
Figure 4.2 Agar gel electrolyte containing 10mM of glucose.

For the assembly of EBFC Patch unit, the agar gel electrolyte is placed in between the GOx anode and Type 1/2 cathode with wires connected for measurement, forming a sandwich geometry.

Figure 4.3 Photograph of a fully operational EBFC patch unit.

As shown in Figure 4.3, the fully operational EBFC patch unit consists of GOx anode, Lac cathode and agar gel electrolyte in a sandwiched geometry with polymer packaging and wiring for external circuit connection.

4.2 Test Results and Discussion

To examine the performance of EBFC patch, several units were fabricated and assembled as shown in Figure 4.4. The electrochemical performance of these units were evaluated by calculating the power output, power densities and analyzing the polarization curves.

Figure 4.4 The EBFC patch unit test apparatus.

Power is calculated by using Equation 4.1, and power density (POD) is determined by using Equation 4.2 where A is the effective area of EBFC electrode. J is the current density.

$$P = VI \qquad\qquad (4.1)$$

$$POD = P/A \qquad\qquad (4.2)$$

$$J = I/A \qquad\qquad (4.3)$$

Several types of EBFC units have been prepared to find the optimal configuration. Three of them were chosen to be discussed due to their good performance. The first biofuel cell labeled BFC 2 was set up in accordance with the design in Figure 4.5(A),

with a glucose concentration of 5 mM in PBS. Enzyme immobilization on the nanopaper

electrodes was carried out by manual compression of the enzymes on the nanopaper.

The maximum power density obtained is $39.44\mu W/cm^2$. The preparation of BFC 3 was

similar to BFC 2, the only difference is that instead of using hand compression, a

hydraulic compressor with 10 metric ton load was employed. BFC 3 showed a maximum

power density of 73.22 $\mu W/cm^2$, which was almost twice that of BFC 2. The highest

power output was observed at 1000Ω load. Hence, an increased pressure, during the

immobilization process of the EBFCs, plays a positive role in the above experiments.
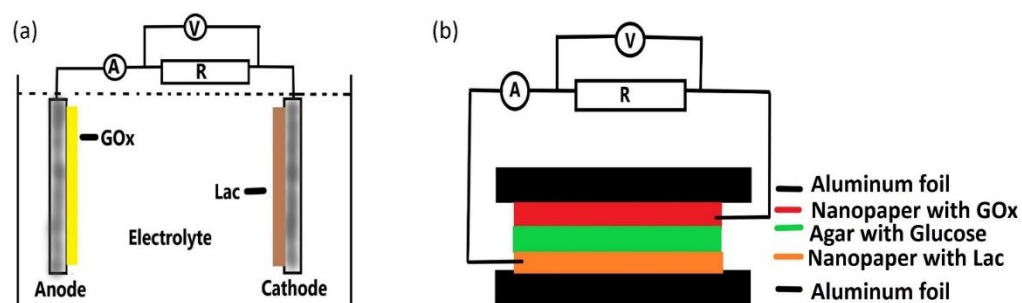
Figure 4.5 Biofuel cell setup and architectures: (A) Set-up 1 showing a conventional biofuel cell, and (B) Set-up 2 showing the sandwich architecture investigated in this study.

BFC 5 was prepared as a sandwich structure (EBFC) as shown in Figure 4.5 (B)

to compare the performance of this EBFC patch form with conventional devices. The

amount of enzyme and glucose concentration is the same. The hydraulic pressure is 10

metric tons which is the same as BFC 3. The highest power output obtained for this

design was $111.90\mu W/cm^2$, at a current density of 334.5 $\mu A/cm^2$, and a voltage of

0.335V. Open circuit potential was observed at 0.869V. BFC 5 exhibited the highest

power output.
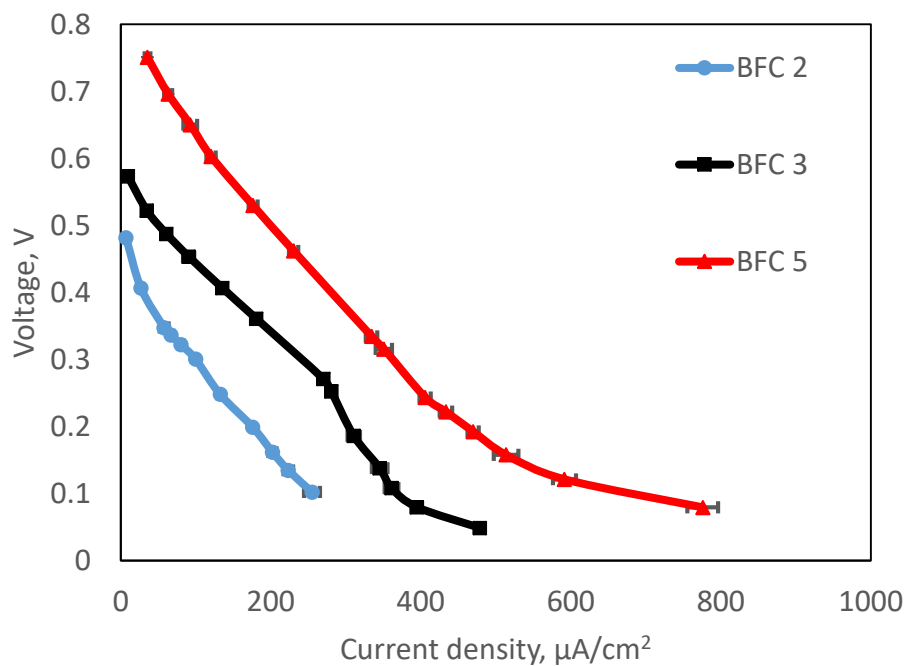
Figure 4.6 Comparison of the polarization (voltage vs current density) curves for BFC 2, 3 and 5.
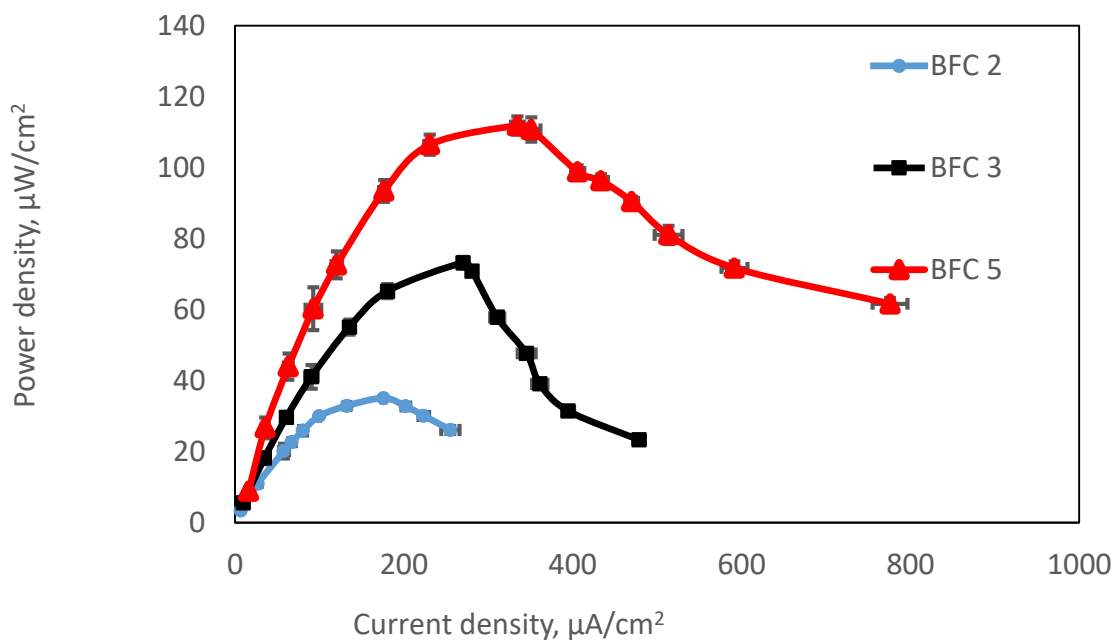
Figure 4.7 Comparison of the power density versus current density curves for BFC 2, 3 and 5.

52

Figures 4.6 and 4.7 show the differences in polarization curves and power density versus current density curves between these three configurations. The error bars show the standard deviation from the mean value of current densities for 3-5 independent experiments. The maximum error is below 10%; these EBFC configurations maintain consistent performance among different test runs. From the above result, it can be concluded that BFC5 shows the best performance among these configurations.
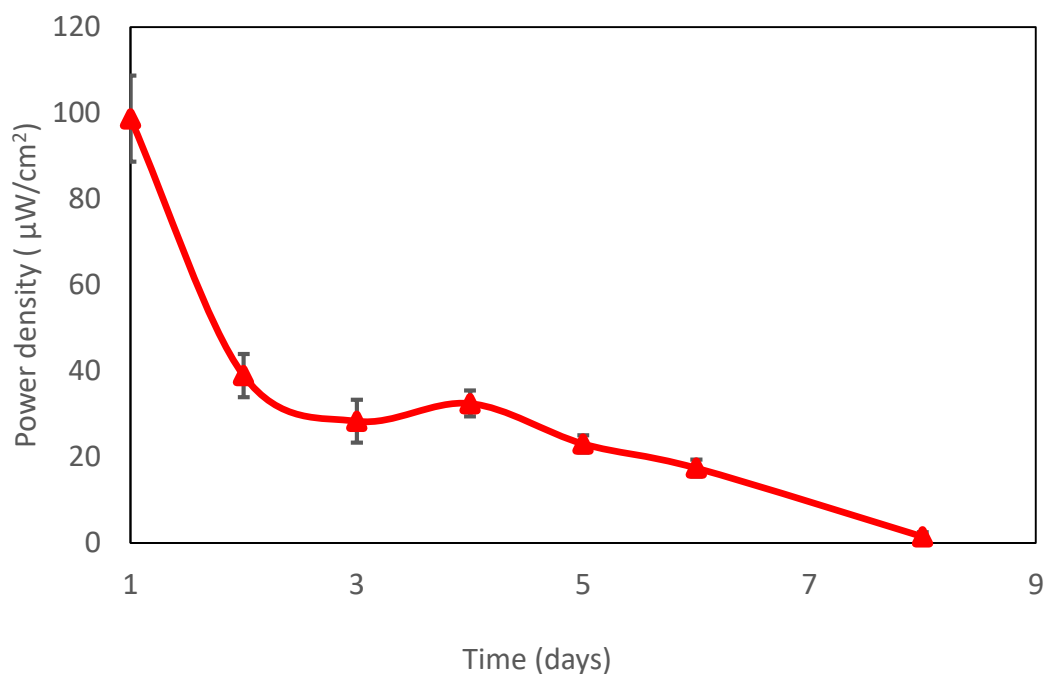
Figure 4.8 Plot of power density versus time in days under load for BFC 5.

The life time of BFC 5 output power versus time measurements (Figure 4.8) shows a significant drop after the first 24 hours probably due to loss of glucose and moisture in the gel electrolyte. Extra water and glucose were added after 3 days, which resulted in an increase in power for about half of a day before BFC 5 eventually lost all power

after 8 days of operation. The error bars show the standard deviation from the mean value of current densities for three independent experiments. Even though a life time of over a week can be expected from BFC 5, the life expectancy of conventional EBFC made in accordance with Figure 4.5(A), can reach about a month of operation time. The main reason for such difference is due to the gel electrolyte. The gel electrolyte, in this case, agar gel tends to loose water in just a few days of operation whereas in conventional design, the aqueous electrolyte has no such issue. Also, the body of agar gel contains much less glucose than aqueous electrolyte because of the big difference in volume. Thus, the dried up agar gel needs to be replaced with fresh moisture-rich new agar gel. The process of such replacement can harm the performance of EBFC which can be identified from the difference in power density of initial and right after replacement of the gel. During the replacement procedure, certain amount of enzyme can be observed in the dried up agar gel which implies some loss of catalyst on the electrodes.
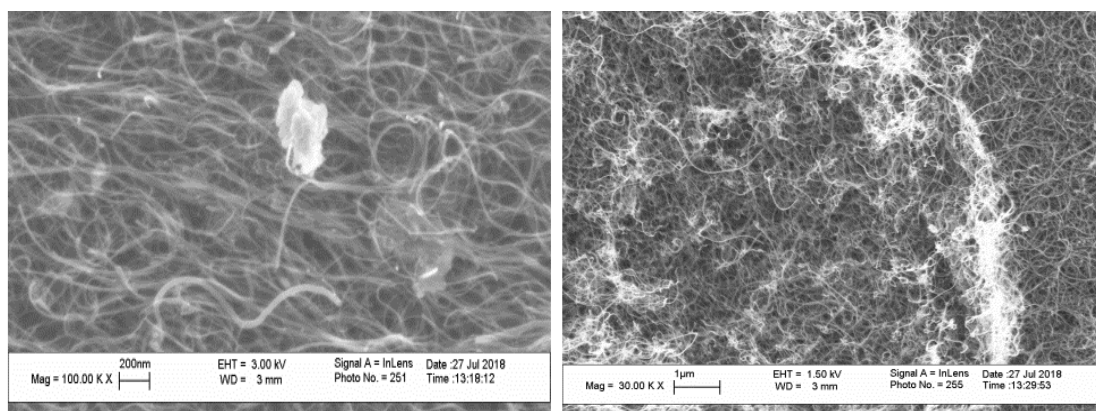
Figure 4.9 SEM images of GOx anode before the EBFC assembly for performance test.
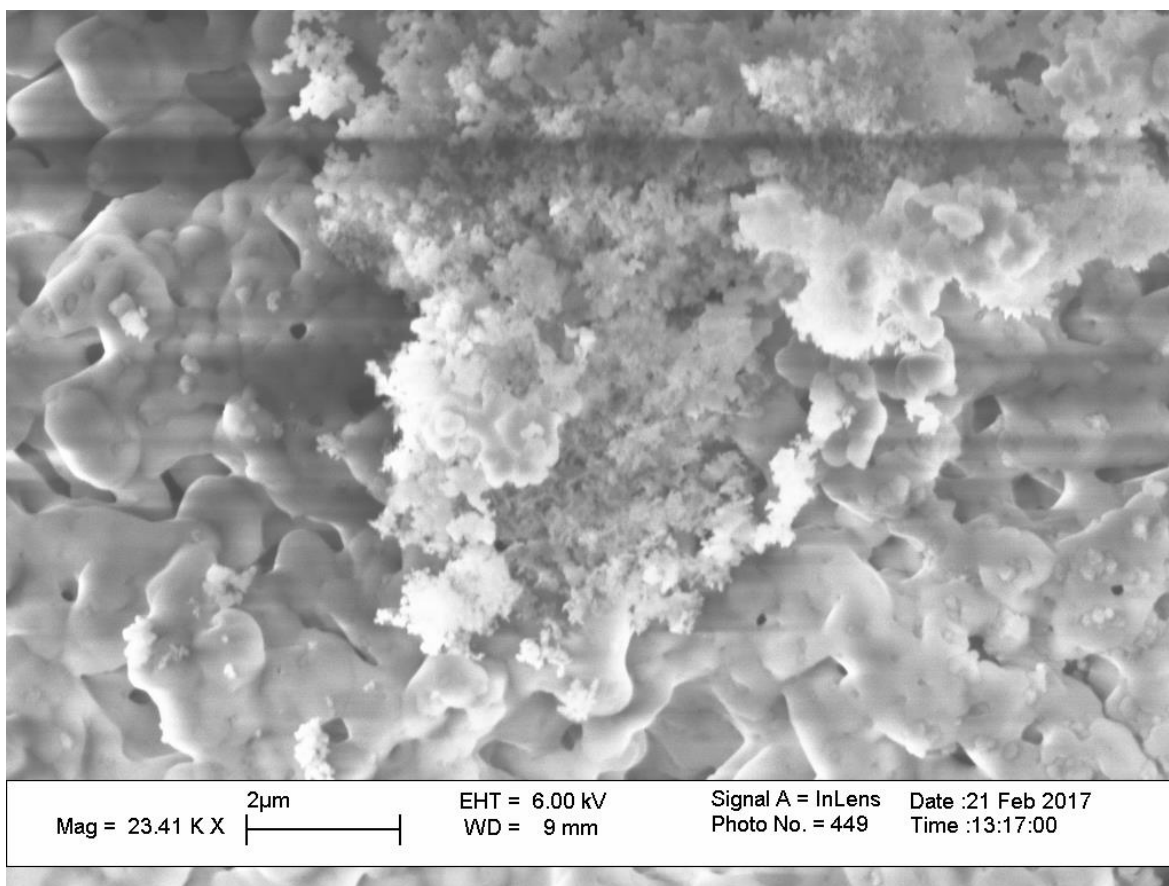
Figure 4.10 SEM image of the GOx anode after EBFC lifetime performance test.

SEM is a good tehcinique to examine the mophorlogy of the surface of a sample. To help better understand the reason for the decrease in power density, Field emission SEM images have been taken. Figure 4.9 shows the Field emission SEM images of the surface of nanopaper GOx anode after compression before EBFC performance test at high magnification (left) and lower magnification (right). These field emission SEM images of the GOx anode showing a relatively uniform distribution of GOx on the CNT nanopaper. These results are similar to those observed by Zebda et al. [106] who also utilized mechanical compression as the immobilization technique.

Figure 4.10 shows the field emission SEM image of another GOx anode which

was fabricated under similar protocol but was assembled into a full EBFC apparatus and the image was extracted after performing lifetime test for more than a week. From this SEM image, it can be observed that the surface of GOx anode has been significatly damaged after the test. There is no sign of wire-like CNT; also, the visibility GOx is poor. Moreover, the SEM run itself was a very difficult one to do, due to the poor conductivity of the electrode. From Equations 1.11 and 1.12, during the oxidation reaction on GOx active site, hydrogen peroxide is produced, which can damage both GOx enzyme and the –COOH function group on the MWCNTs. It is also believed that the presence of hydrogen peroxide has negative effect on laccase performance[108] which was on the cathode. Figure 4.10 can be regarded as a proof of such redox reaction mechanism. More evidence of the presence of hydrogen peroxide is presented in Appendix B using a SERS measurement.

4.3 Hybrid EBFC Patch

By combining GOx anode with non-biological cathode to fabricate a hybrid EBFC has led to good results in as early as 1998 by Palmore et al. They utilized methanol MET anode with Pt cathode and produced a BFC with highest current density of 2600 $\mu A/cm^2$ and power density of 680 $\mu W/cm^2$[109]. Later, more research has been perfomed regarding this concept of utilizing a bioanode with a non-biological cathode to fabricate a hybrid EBFC. Akers et al. used ethanol MET anode and Pt cathode; they obtained a BFC with much lower current density of 3 to 5.4 $\mu A/cm^2$ but maximum power density ranging from 1160 to 2040 $\mu W/cm^2$ [103]. Arechederra et al. used glycerol DET anode and Pt cathode to develop a BFC with current density of 4200 $\mu A/cm^2$ and power density

of 1210 $\mu W/cm^2$ [110]. Zhu et al. used Maltodextrin MET anode and Pt cathode to develop a BFC which yielded a maximum current density of 6000 $\mu A/cm^2$ and power density of 800 $\mu W/cm^2$ [111]. The open circuit voltage of these BFCs range from 0.65V to 0.8V. From these examples, Pt has been considered to be a good choice for non-biological cathode because of the good stability and the higher potential difference from the anode than other bio-cathodes. Also, Pt can serve as a catalyst in the decomposition of hydrogen peroxide [112] which is produced in the oxidation reaction of glucose by GOx; it is an excellent choice for cathode material.

In light of the previous progress, novel hybrid EBFC patches have been designed and fabricated for research purposes. Two types of hybrid EBFC patches have been fabricated.

The first type of hybrid EBFC patch consists of GOx anode that is constructed the same way as it was previously. The non-biological cathode is fabricated with two methods. Method 1 is as follows: platinum on graphitized carbon (10wt% loading, from Sigma-Aldrich) is mixed with Nafion® solution and dropped on premade CNT nanopaper followed by annealing in an oven at 90°C for 1 hour.

Instead of drop casting the mixture of Pt carbon Nafion solution, method 2 utilizes a mixture of Pt carbon powder with carbon nanotubes (MWCNTs) (Carbon Solutions Inc.), sodium dodecyl sulfate (SDS) and phosphate buffer of pH 7.4. The mixture is sonicated at conditions of 75% amplitude, for 30 minutes at a pulse of 30 seconds with 10 seconds interval and filtered by vacuum filtration for the formation of nanopaper. The filter papers used are of 10μm pore size. Filter papers are dipped in 10ml ethanol for 10 min before the vacuum filtration. The nanopapers are washed with 100 ml DI

water at 95°C for couple of hours to remove the residue particles.

The hybrid EBFC patch was prepared by using the same EBFC patch sandwich model with agar placed in between the two CNT nanopapers with electrodes which were connected to wires for power output measurements. The patch unit was placed in a plastic box.

Then the EBFC patch was taken and heated at a temperature of 25 to 27°C on a hot plate. Agar and glucose act as power sources of the cell. Current density and voltage were calculated using the measured current and voltage, from ammeter and voltmeter, respectively, at regular intervals by changing the load resistance.

The GOx-Pt patch unit#1 was prepared using method 1. The open circuit voltage of this unit reached 0.8V. The power density is $112.2\mu W/cm^2$ at maximum in the beginning, but then it drops significantly in a few hours. 60 hours later, some post buffered solution (PBS) with glucose was dropped in the unit in order to increase the power. However, unit#1 stopped working after around 80 hours of lifetime.
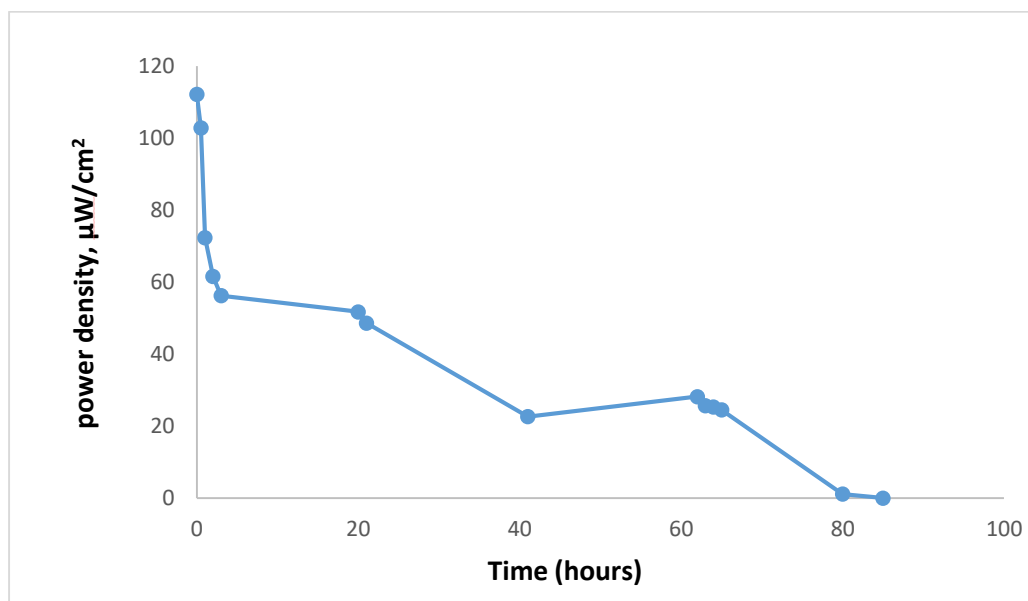
Figure 4.11 Power density vs time of GOx-Pt EBFC unit#1.

The GOx-Pt patch unit#2 was prepared with method 2. The open circuit voltage of this unit reached 0.9V. The power density was 146.01μW/cm^2 at maximum in the beginning, but it decreased significantly in a few hours. 45 hours later, some PBS with glucose was dropped in the unit to increase the power. The power density decreased after an initial increase. Eventually, unit#2 stopped working after ~150 hours.
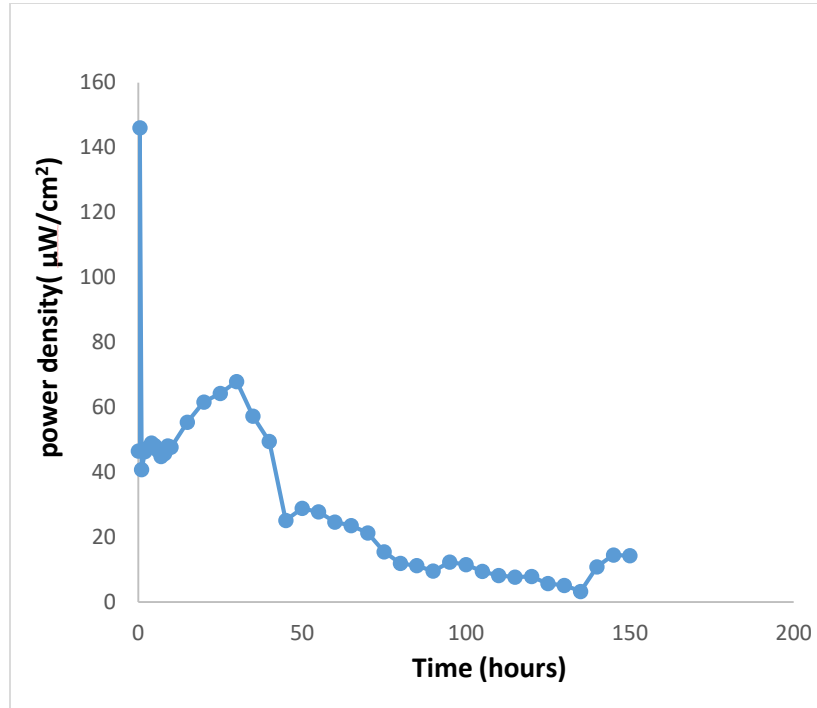
Figure 4.12 Power density vs time of GOx-Pt EBFC unit#2.

By comparing the two units, the GOx-Pt EBFC patch unit#2, which was fabricated with method 2, shows not only a higher open circuit voltage and maximum power density, but also a better lifetime performance.

Comparing the maximum power density of hybrid EBFC patch with EBFC patch, the hybrid EBFC exhibits better performance; however, the life time performance is not as good as the EBFC patch which uses Lac as the cathode catalyst.

200nm   EHT = 6.00 kV   Signal A = InLens   Date :21 Feb 2017
Mag = 75.00 K X   ⊢—⊣   WD = 8 mm   Photo No. = 443   Time :12:53:01
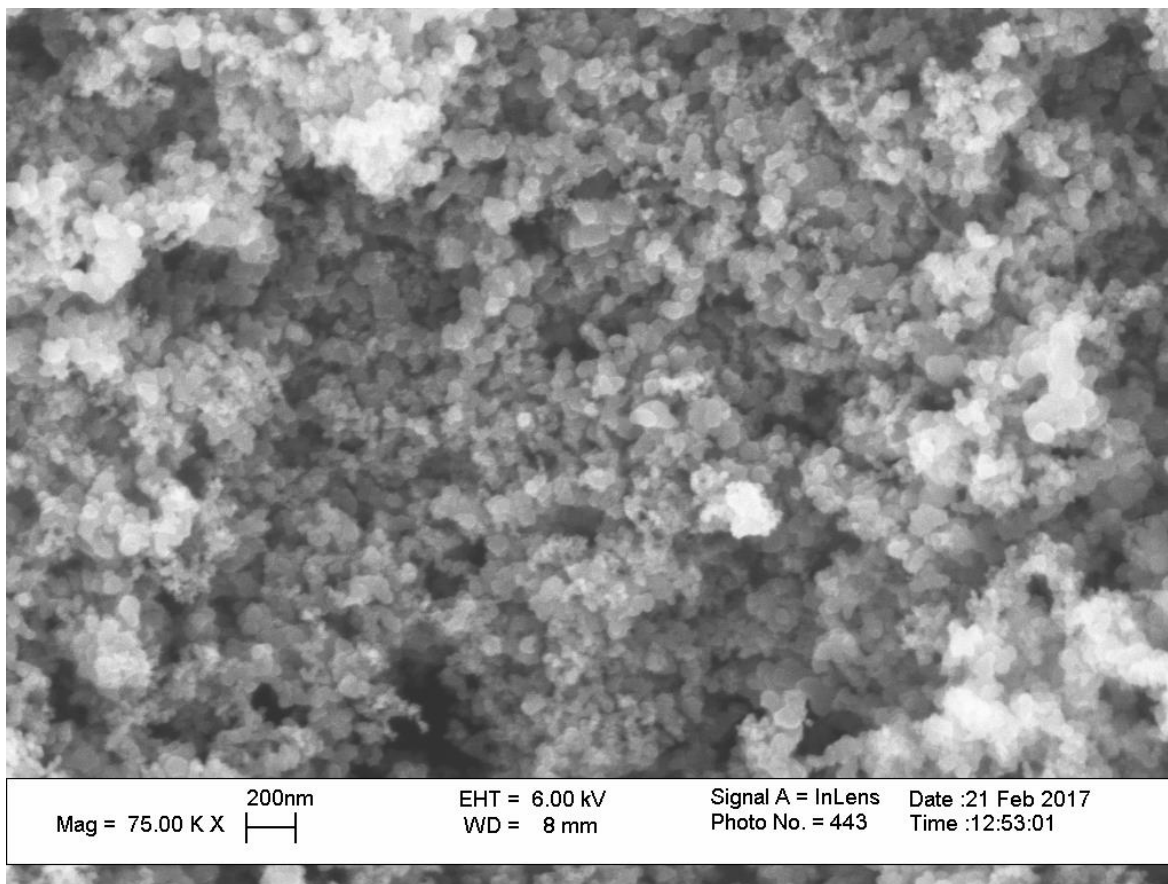
Figure 4.13 SEM image of a fresh Pt-CNT cathode made with method 2.

Figure 4.13 shows the SEM results of Pt-CNT cathode. From this figure, the morphology of the surface of such sample is completely different from the surface of a simple CNT nanopaper. The uniform distribution of Pt on CNT nanopaper can be observed. Figure 4.14 shows the SEM image of a used Pt-CNT cathode made with method 2. The differences between a fresh and Pt-CNT cathode can be easily observed. Big clusters of hydrocarbon produced after the redox reactions can be seen on the surface blocking Pt causing a significant decrease in power density in the hybrid EBFC patch. Similar phenomenon has been observed and reported previously [113]. Another possible source of such contaminants is due to Nafion® membrane [114].
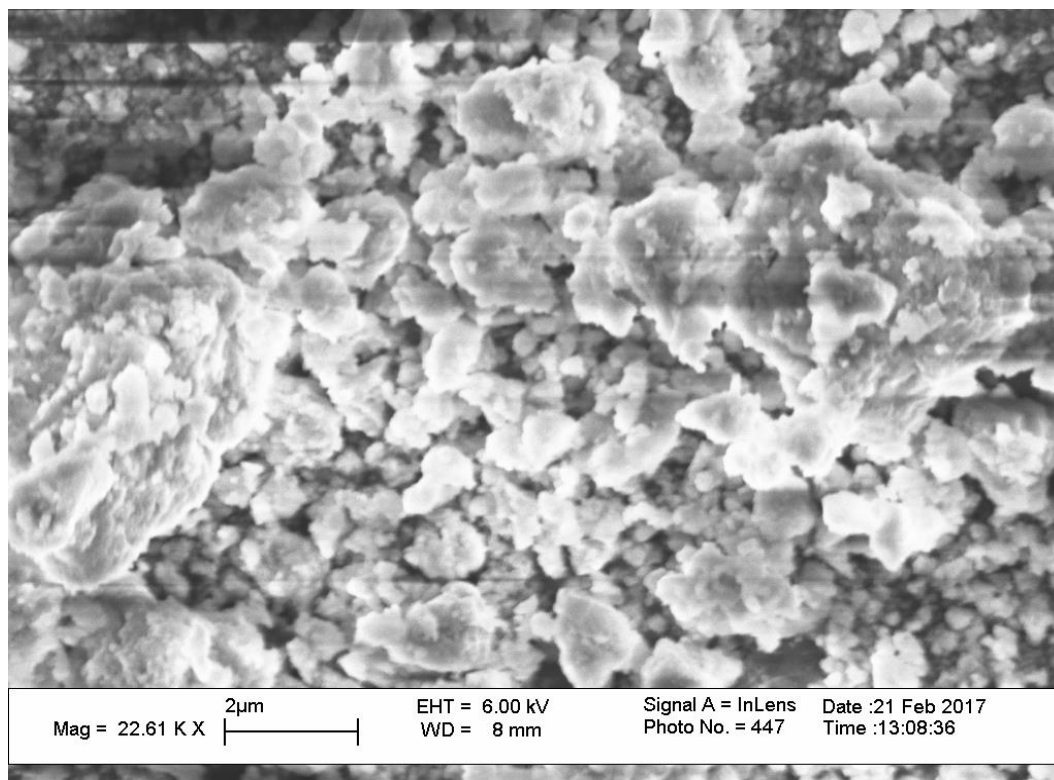
Figure 4.14 SEM image of a used Pt-CNT cathode made with method 2.
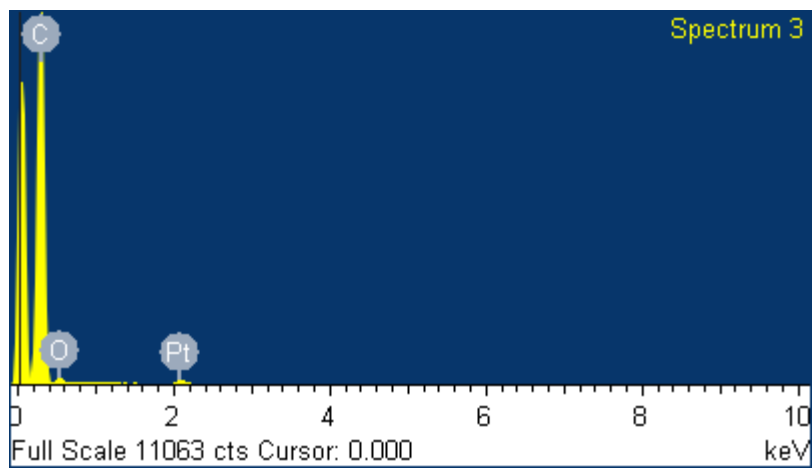
Figure 4.15 EDS measurement of Pt-CNT cathode sample made with method 2.

Table 4.1 Weight% of Pt-CNT Cathode Sample Made with Method 2

Element	Weight%	Atomic%
Carbon	89.70	97.34
Oxygen	2.63	2.14
Platinum	7.67	0.51
Totals	100.00	

Figure 4.15 and Table 4.1 show the EDS results of the same Pt-CNT cathode sample. From these results, the weight% of Pt of the surface of the cathode is over 7 weight% which agrees with the SEM results showing a thorough coverage of Pt on the nanopaper.

4.4 Hybrid EBFC Patch in Series

With the feasibility of the concept of hybrid EBFC patch having been examined successfully, a question of 'can it be arranged in series to increase the power' arises naturally. In order to answer the question, this section presents the results of two hybrid EBFC patch units made from method 2 that were assembled in series. These two hybrid EBFC patch units were assembled at the same time and in the same manner to form identical units. The agar gel preparation is in accordance with the same protocol. The ambient temperature of the experiment is around 22-23°C. This experiment mainly focused on the power generation performance; thus the running time is about 3 hours considering the previously observed sharp drop in power density within the first few hours of operation of hybrid EBFC patch units.

Figure 4.16 Two identical hybrid EBFC patch units in series.

As Figure 4.16 shows, the unit#1 (left) and unit#2(right) were assembled in series. The active area ($0.6cm^2$) was controlled in a 5mm by 12mm rectangle on both GOx anode and Pt-CNT cathode. The resistor was set at 1000ohm (Figure 4.17 left) to achieve maximum power output. At peak performance, the maximum power density calculated is $0.574mW/cm^2$ at 0.83V and 0.83mA (Figure 4.17) for this apparatus. This is by far the highest power density that has been achieved in this configuration of hybrid EBFC patch design. It increased the maximum power density of a single hybrid EBFC patch by four times.
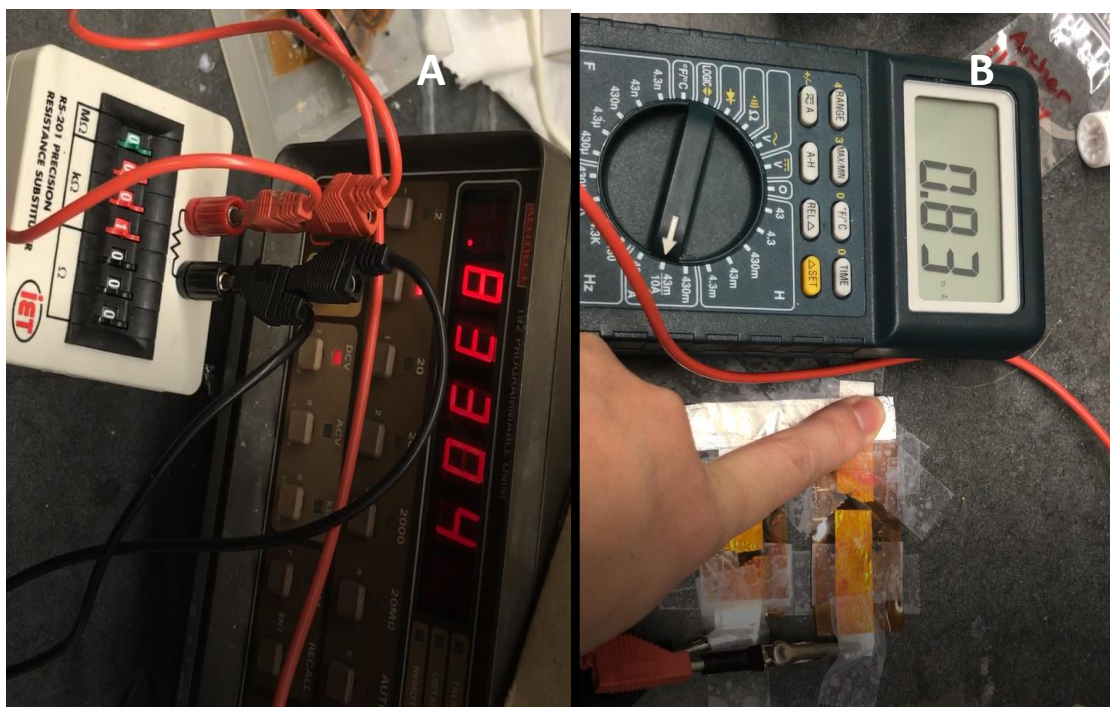
Figure 4.17 Voltage (left) and current (right) measurement of two identical hybrid EBFC patch units in series under 1k ohm load.

This experiment shows the improved performance of hybrid EBFC patch compared to EBFC patch unit using Laccase as the cathode catalyst. It also demonstrates the feasibility of one common approach of utilizing multiple low power battery units in series as a whole module to increase the power. More importantly, this concept can be utilized in the design of EBFC patch, which is very difficult to do with the conventional EBFC [115, 116].

CHAPTER 5

SUMMARY AND FUTURE DIRECTIONS

5.1 Summary

Enzyme compression on CNT nanopaper electrodes is a new and promising technique used for biofuel cell fabrication. This has various advantages over other immobilization techniques. In this dissertation, commercially available MWCNTs were purchased for the fabrication of electrode base material. GOx and Laccase were used as biocatalysts for the fabrication of EBFCs and Pt was used as the cathode catalyst for the hybrid EBFC patch design. Mechanical compression was utilized in the fabrication process of bio-electrodes and Pt cathode. The bio-electrodes prepared with compression technique was set up in a conventional EBFC apparatus for the performance tests. The test results show good power density and current density along with over-one-month stability. The patch form EBFC, with the same bio-electrodes, was developed and tested with the use of agar gel electrolyte. This patch form design shows good power density and current density along with over-one-week lifetime performance. Agar plays a major role in determining the life expectancy of the biofuel cell when a sandwich geometry is used. However, methods need to be developed to prevent Agar from forming a hard gel which interrupts the electric conductivity in the sandwich as well as for better power output. Hybrid EBFC such as GOx-Pt EBFC patch unit has been developed for the first time. Two different preparation methods of Pt-CNTs cathode has been tested. The second method with the use of vacuum filtration system shows not only a higher open circuit voltage and maximum power density, but also a better lifetime performance. Compared to

normal EBFC patch, the test results show a higher maximum power density and open circuit voltage, but the life time performance is considerably lower. Factors including hydrogen peroxide build up causing the poisoning of GOx anode and a faster rate of hard gel formation could be the reasons for this decreased performance. A hybrid EBFC patch, in series, demonstrates the feasibility to stack up multiple units in order to achieve higher power output. The initial results are impressive with an increase in the maximum power density by four times.

It can be concluded that the mechanical compression technique for enzyme immobilization is a feasible solution but requires further fine tuning. The EBFC patch design demonstrates a path with good potential for commercially viable products that can be cost-effectively fabricated in a facile manner to produce wearable and potentially disposable power devices. These devices can provide performance levels that are comparable to that of most conventional biofuel cells.

5.2 Future Directions

The following factors need to be addressed to improve the performance of the proposed approach. The average life time of EBFC patch form is significantly shorter than that of conventional EBFC. Even though the maximum power density of EBFC patch units is higher than that of conventional EBFC, the decrease in power density in patch unit is much faster, especially with the hybrid EBFC patch using Pt-CNT as cathode.

A preliminary result of SERS measurement is presented in Appendix B indicating the formation of hydrogen peroxide on GOx anode. Real-time in-situ monitoring of EBFC via fiber optic probe Raman spectroscopy can help to further study the

mechanisms of overall redox reactions in EBFC and help to discover the reason for rapid decease in power density. In Appendix D, some different materials has been tested for the fabrication of CNT nanopaper, strategies can be implemented for further improvements such as to identify different functional group with CNT or metallic compound to help establish better DET pathways and higher rates. Also, one can test SWCNTs with different lengths to help the immobilization procedure which may increase the lifetime performance of EBFCs. Simulation and modeling via COMSOL MULTIPHYSICS can help to improve the bio-electrode design.

Some other strategies can be implemented in the preparation of a cell which can be implanted into the human body with agar and glucose acting as the power sources. Also, a commercial viable wearable form of the EBFC patch module consisting of multiple units can be developed with flexible electrode base material and polymer film for packaging.

APPENDIX A
PREPARATION OF GLUCOSE OXIDASE ANODE FOR SURFACE-ENHANCEMENT RAMAN SPECTROSCOPY

The following appendix discusses the preparation of GOx anode for Surface-Enhancement Raman Spectroscopy (SERS).

Chemicals and reagents that were used for the preparation of SERS samples are listed below (All chemicals and reagents were analytical grade or higher and used as received without further purification). Gold (III) chloride trihydrate (99.9%), dehydrated sodium citrate (99%), and anhydrous 96% alpha D-glucose 96% were purchased from Sigma-Aldrich. Graphene-like sheets were obtained from Graphene Laboratories Inc. Tri(ethylene glycol)mono tri(ethylene glycol)-11-mercaptoundecul ether, 95% was purchased from Sigma-Aldrich.

The preparation of gold nanoparticles: Gold nanoparticles were prepared by reduction of gold (III) chloride trihydrate with sodium citrate as described by Turkevish [117] and Ferns [118]. Briefly, an aqueous solution of gold (III) chloride trihydrate (0.5M, 25 ml) was heated to 98°C. It was then stirred and 1 ml of 1% aqueous sodium citrate solution was added to it. The mixture obtained was kept at 95°C and then continuously stirred for 30 minutes to give a dark red solution. Then, gold nanoparticles with concentration (0.04 M) were deposited on the previously prepared CNT nanopapers.

Preparation of glucose solutions: Glucose was added into PBS to form a glucose solution with concentrations of 0.1M for the use of SERS measurements.

SURFACE-ENHANCEMENT RAMAN SPECTROSCOPY MEASUREMENT
OF GLUCOSE OXIDASE ANODE

Hence are the preliminary results and discussion of the measurement of SERS of GOx anode.
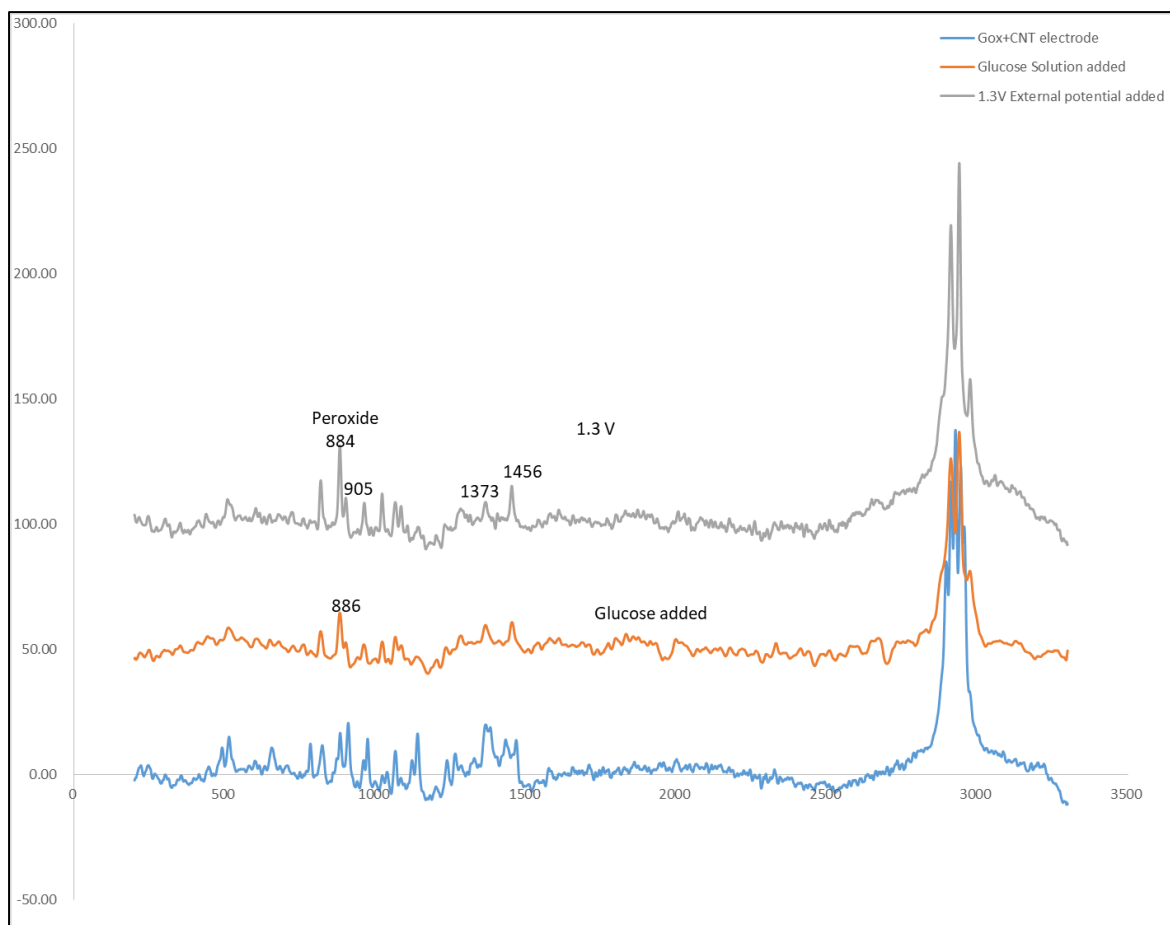
Figure B.1 Comparison of SERS of the same GOx anode under different conditions.

The blue line shows the SERS of the free standing GOx anode. The orange line shows the SERS of the same GOx anode after adding few drops of PBS (pH 7.4, containing 0.1M glucose) allowing the presence of glucose on the GOx anode surface while not too wet preventing a readable data for the Raman instrument. The gray line

represents the same GOx anode sample, but an external circuit was established using a

1.3V AAA batteries after the previous introduction of glucose containing PBS. Its

function is to simulate the *vivo* operation electrochemical environment of a running

EBFC. With the potential of 1.3 volts added, the line at 884 cm^{-1} and a companion line

at 920 cm^{-1} associated with hydrogen peroxide grew in intensity [119]. Changes in the

conformation of GOx around the CH bonds also occur because of the increase in

intensity of the lines at 820 and 1456 cm^{-1} which can be assigned to CH deformation

modes in GOx [120].

APPENDIX C

24 HOUR MONITORING SYSTEM FOR THE EBFC PERFORMANCE

In order to measure the performance of EBFC power over time (lifetime), constant monitoring is required. In order to automate the measurements over long durations, a 24-hour monitoring system was established. The system consists of hardware and software setup. A PC with a dedicated camera is needed for the hardware setup (Figure C.1).
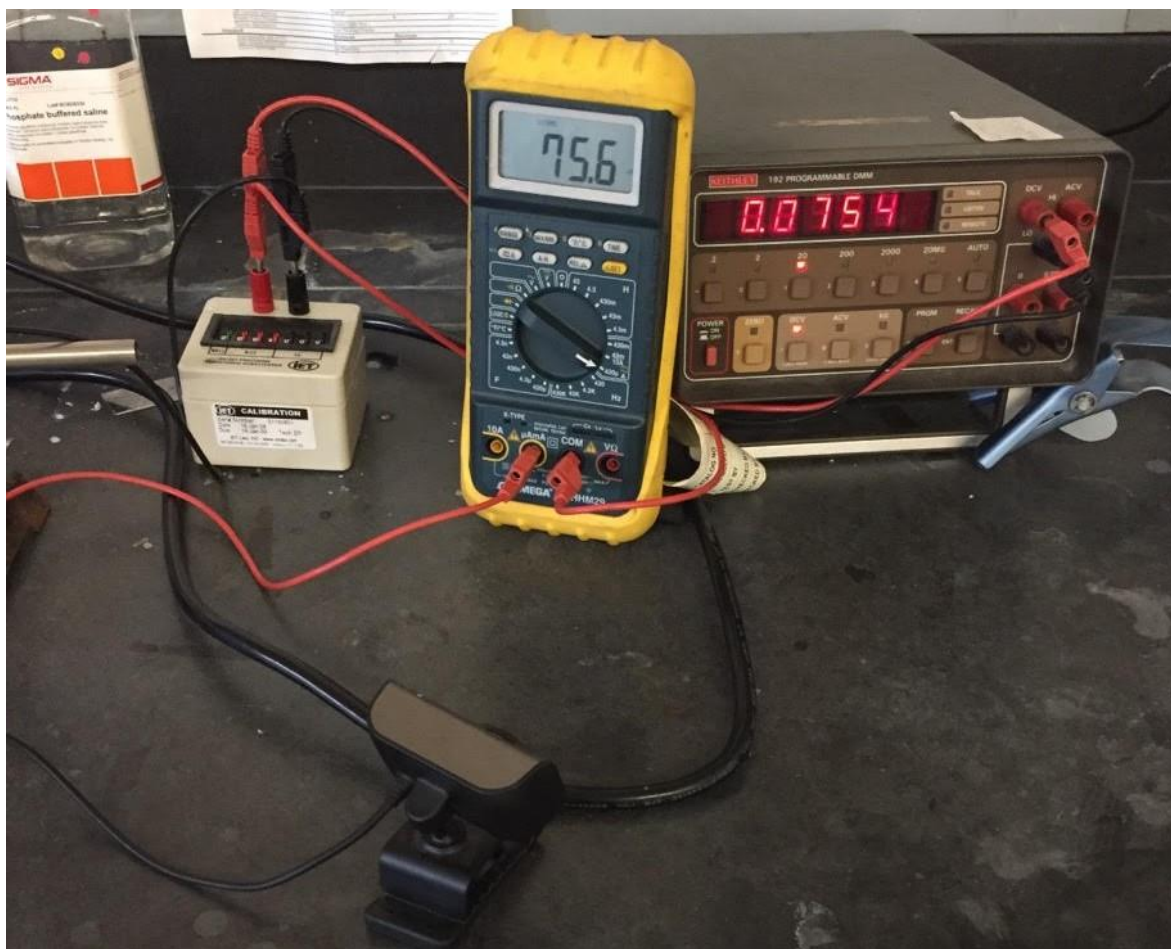
Figure C.1 24-hour monitoring system setup.

A program coded with Python 3.0 was used for the software setup. The principle idea of this program is to construct a video monitoring of EBFC setup while capturing the snapshot of the video at a certain frequency allowing consistent monitoring of the EBFC performance while not exceeding the limitation of hard drive storage. The following is the Python code of such program.

```
#!/usr/bin/env python
# -*- coding: utf-8 -*-


from VideoCapture import Device
import time


#Maximum number of picture can be captured.
MAX_PIC_NUM = 2016


#Frequency of picture capture. One picture every 300 seconds in following case.
SLEEP_TIME_LONG = 300


cam = Device(devnum=0, showVideoWindow=0)


iNum = 0
while True:


    #Snapshot of video stream.
```

```python
        cam.saveSnapshot(str(iNum)+ '.jpg', timestamp=3, boldfont=1, quality=75)


        time.sleep(SLEEP_TIME_LONG)


#Overwrite if the maximum number reached
    if iNum == MAX_PIC_NUM:

        iNum = 0

    else:

        iNum += 1
```

APPENDIX D

OTHER EXPERIMENTS CONDUCTED IN THE DISSERTATION

In addition to the project of this dissertation, other projects have been undertaken to examine the possibility of replacing certain materials for improved performance.

One of the projects is to design a configuration of hybrid EBFC by using Polynitrogen (PN) as cathode for the oxidation reduction reaction replacing Pt and Laccase.

To synthesize the PN oligomer N_8^- on positively charged MWCNTs, cyclic voltammetry (CV) was carried out under 245 nm UV irradiation using a computer-controlled CH Instruments 832C potentiostatgalvanostat on -COOH functionalized multi-walled carbon nanotubes (MWCNTs, purchased from Nanolab, Inc). CV was performed with a three-electrode setup. The working electrode was dipped in 40 mL 0.5–4m NaN_3 (Aldrich) and dissolved in a buffer solution (pH 4.0). This was used as the electrolyte. Pt and Ag/AgCl were used as the counter electrode and standard reference electrode, respectively. CV was also carried out on MWCNT-glassy carbon electrode (GCE) without NaN_3 in the solution to clarify the oxidation peak from N_3^- [121].

A PN hybrid EBFC apparatus was prepared in accordance with the conventional EBFC setup except replacing the laccase cathode with a PN cathode. The power density versus time plot is presented in Figure D.1. The power output, although much lower than the both conventional EBFCs and the Pt hybrid EBFC, had a respectable half-life of over 40 hrs. Power output measurements were repeated several times but the outputs did

not exceed 4.5 micro-Watts/cm^2. Therefore, the approach of utilizing a PN cathode to fabricate hybrid EBFC was not pursued further and will have to await for the optimization of this novel catalyst.
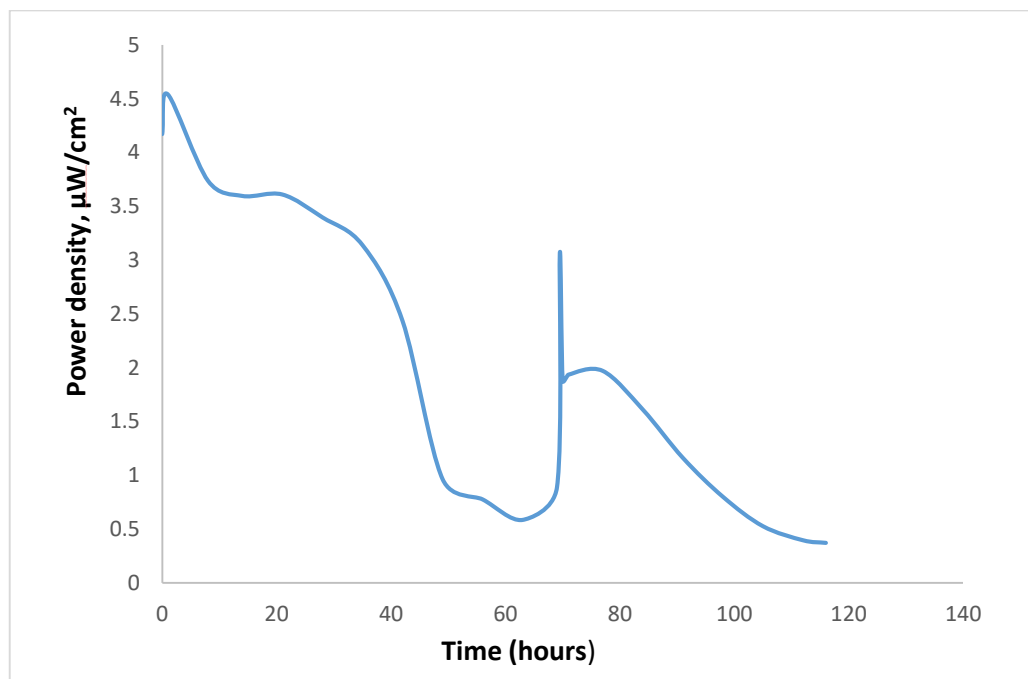
Figure D.1 Power density versus time of GOx-PN hybrid EBFC.

REFERENCES

1.   *BP Statistical Review of World Energy*. [cited 2018 August 30th];Available from: https://www.bp.com/content/dam/bp/en/corporate/pdf/energy-economics/statistical-review/bp-stats-review-2018-full-report.pdf.

2.   Grove, W.R., *XXIV. On voltaic series and the combination of gases by platinum.* The London, Edinburgh, and Dublin Philosophical Magazine and Journal of Science, 1839. **14**(86-87): p. 127-130.

3.   Steele, B.C.H. and A. Heinzel, *Materials for fuel-cell technologies*, in Materials for Sustainable Energy. p. 224-231.

4.   *Fuel cell*. [cited 2018 August 30th];Available from: http://butane.chem.uiuc.edu/pshapley/Enlist/Labs/FuelCellLab/FuelCell.html.

5.   Wiyaratn, W., *Reviews on fuel cell technology for valuable chemicals and energy co-generation.* Engineering Journal, 2010. **14**(3): p. 1-14.

6.   Allen, R.M. and H.P. Bennetto, *Microbial fuel-cells.* Applied Biochemistry and Biotechnology, 1993. **39**(1): p. 27-40.

7.   Rahimnejad, M., G. Najafpour, and A.A. Ghoreyshi, *Effect of mass transfer on performance of microbial fuel cell*, in Mass Transfer in Chemical Engineering Processes. 2011, InTech.

8.   *Electrical effects accompanying the decomposition of organic compounds.* Proceedings of the Royal Society of London. Series B, Containing Papers of a Biological Character, 1911. **84**(571): p. 260-276.

9.   Logan, B.E., et al., *Microbial Fuel Cells: Methodology and Technology.* Environmental Science & Technology, 2006. **40**(17): p. 5181-5192.

10.   Bond, D.R., et al., *Electrode-Reducing Microorganisms That Harvest Energy from Marine Sediments.* Science, 2002. **295**(5554): p. 483-485.

11.   Rahimnejad, M., et al., *Low voltage power generation in abiofuel cell using anaerobic cultures.* World Applied Sciences Journal, 2009. **6**(11): p. 1585-1588.

12.   Zhou, M., et al., *Microbial fuel cells for bioenergy and bioproducts*, in Sustainable Bioenergy and Bioproducts. 2012, Springer. p. 131-171.

13.   Nevin, K.P., et al., *Power output and columbic efficiencies from biofilms of Geobacter sulfurreducens comparable to mixed community microbial fuel cells.* Environmental Microbiology, 2008. **10**(10): p. 2505-2514.

14.   Zou, Y., et al., *A mediatorless microbial fuel cell using polypyrrole coated carbon nanotubes composite as anode material.* International Journal of Hydrogen Energy, 2008. **33**(18): p. 4856-4862.

15.   Sharma, Y. and B. Li, *The variation of power generation with organic substrates in single-chamber microbial fuel cells (SCMFCs).* Bioresource Technology, 2010. **101**(6): p. 1844-1850.

16.   Rasmussen, M., S. Abdellaoui, and S.D. Minteer, *Enzymatic biofuel cells: 30 years of critical advancements.* Biosensors and Bioelectronics, 2016. **76**: p. 91-102.

17.   Yahiro, A., S. Lee, and D. Kimble, *Bioelectrochemistry: I. Enzyme utilizing bio-fuel cell studies.* Biochimica et Biophysica Acta (BBA)-Specialized Section on Biophysical Subjects, 1964. **88**(2): p. 375-383.

18.   Katz, E., A. Shipway, and I. Willner, *Handbook of fuel cells—fundamentals, technology and applications.* Fundamentals and Survey of Systems, 2003. **1**: p. 355.

19.   Berezin, I., et al., *Bioelectrocatalysis-Equilibrium oxygen potential in presence of laccase.* Doklady Akademii Nauk SSSR, 1978. **240**(3): p. 615-618.

20.   Cass, A.E.G., et al., *Ferrocene-mediated enzyme electrode for amperometric determination of glucose.* Analytical Chemistry, 1984. **56**(4): p. 667-671.

21.   Dicks, J., et al. *Ferrocene modified polypyrrole with immobilised glucose oxidase and its application in amperometric glucose microbiosensors*. in Annales de Biologie Clinique. 1989.

22.   Le Goff, A., M. Holzinger, and S. Cosnier, *Recent progress in oxygen-reducing laccase biocathodes for enzymatic biofuel cells.* Cellular and Molecular Life Sciences, 2015. **72**(5): p. 941-52.

23.   Scott, K., et al., *4.11 - Biological and Microbial Fuel Cells*, in Comprehensive Renewable Energy, A. Sayigh, Editor. 2012, Elsevier: Oxford. p. 277-300.

24.   Willner, I., et al., *Reconstitution of apo-glucose oxidase with a nitrospiropyran-modified FAD cofactor yields a photoswitchable biocatalyst for amperometric transduction of recorded optical signals.* Journal of the American Chemical Society, 1996. **118**(22): p. 5310-5311.

25.   Heller, A., *Electrical wiring of redox enzymes.* Accounts of Chemical Research, 1990. **23**(5): p. 128-134.

26.   Degani, Y. and A. Heller, *Direct electrical communication between chemically modified enzymes and metal electrodes. I. Electron transfer from glucose oxidase to metal electrodes via electron relays, bound covalently to the enzyme.* Journal of Physical Chemistry, 1987. **91**(6): p. 1285-1289.

27.   Tamaki, T., T. Ito, and T. Yamaguchi, *Immobilization of hydroquinone through a spacer to polymer grafted on carbon black for a high-surface-area biofuel cell electrode.* The Journal of Physical Chemistry B, 2007. **111**(34): p. 10312-10319.

28.   Bohmhammel, K., et al., *Calorimetric investigations into enzyme catalysed glucose oxidation.* Thermochimica Acta, 1993. **217**: p. 1-7.

29.   Katz, E., et al., *Reconstitution of the quinoprotein glucose dehydrogenase from its apoenzyme on a gold electrode surface modified with a monolayer of pyrroloquinoline q.* Journal of Electroanalytical Chemistry, 1994. **368**(1-2): p. 165-171.

30.   Willner, I., G. Arad, and E. Katz, *A biofuel cell based on pyrroloquinoline quinone and microperoxidase-11 monolayer-functionalized electrodes.* Bioelectrochemistry and Bioenergetics, 1998. **44**(2): p. 209-214.

31.   Xiao, Y., et al., *" Plugging into enzymes": Nanowiring of redox enzymes by a gold nanoparticle.* Science, 2003. **299**(5614): p. 1877-1881.

32.   Katz, E., et al., *Glucose oxidase electrodes via reconstitution of the apo-enzyme: tailoring of novel glucose biosensors.* Analytica Chimica Acta, 1999. **385**(1): p. 45-58.

33.   Yang, S., et al., *Direct electrodeposition of a biocomposite consisting of reduced graphene oxide, chitosan and glucose oxidase on a glassy carbon electrode for direct sensing of glucose.* Microchimica Acta, 2013. **180**(1-2): p. 127-135.

34.   Ivanov, I., T. Vidaković-Koch, and K. Sundmacher, *Recent advances in enzymatic fuel cells: experiments and modeling.* Energies, 2010. **3**(4): p. 803-846.

35.   Wang, S.C., et al., *Membrane-less and mediator-free enzymatic biofuel cell using carbon nanotube/porous silicon electrodes.* Electrochemistry Communications, 2009. **11**(1): p. 34-37.

36.   Katz, E., I. Willner, and A.B. Kotlyar, *A non-compartmentalized glucose/O2 biofuel cell by bioengineered electrode surfaces.* Journal of Electroanalytical Chemistry, 1999. **479**(1): p. 64-68.

37.   Topcagic, S. and S.D. Minteer, *Development of a membraneless ethanol/oxygen biofuel cell.* Electrochimica Acta, 2006. **51**(11): p. 2168-2172.

38.   Kwon, C.H., et al., *High-power biofuel cell textiles from woven biscrolled carbon nanotube yarns.* Nature Communications, 2014. **5**: p. 3928.

39.   Abreu, C., et al., *Glucose oxidase bioanodes for glucose conversion and $H_2 O_2$ production for horseradish peroxidase biocathodes in a flow through glucose biofuel cell design.* Journal of Power Sources, 2018. **392**: p. 176-180.

40.   Shitanda, I., et al., *A screen-printed circular-type paper-based glucose/O_2 biofuel cell.* Journal of Power Sources, 2017. **360**: p. 516-519.

41.   Cosnier, S., A. Le Goff, and M. Holzinger, *Towards glucose biofuel cells implanted in human body for powering artificial organs: Review.* Electrochemistry Communications, 2014. **38**: p. 19-23.

42.   Castorena-Gonzalez, J.A., et al., *Biofuel Cell Operating in-Vivo in Rat.* Electroanalysis, 2013. **25**(7): p. 1579-1584.

43.   Halámková, L., et al., *Implanted Biofuel Cell Operating in a Living Snail.* Journal of the American Chemical Society, 2012. **134**(11): p. 5040-5043.

44.   Rasmussen, M., et al., *An Implantable Biofuel Cell for a Live Insect.* Journal of the American Chemical Society, 2012. **134**(3): p. 1458-1460.

45.   MacVittie, K., et al., *From "cyborg" lobsters to a pacemaker powered by implantable biofuel cells.* Energy & Environmental Science, 2013. **6**(1): p. 81-86.

46.   Jia, W., et al., *Epidermal Biofuel Cells: Energy Harvesting from Human Perspiration.* Angewandte Chemie International Edition, 2013. **52**(28): p. 7233-7236.

47.   Jia, W., et al., *Wearable textile biofuel cells for powering electronics.* Journal of Materials Chemistry A, 2014. **2**(43): p. 18184-18189.

48.   Haneda, K., et al., *Sheet-shaped biofuel cell constructed from enzyme-modified nanoengineered carbon fabric.* Electrochimica Acta, 2012. **82**: p. 175-178.

49.   Ogawa, Y., et al., *Stretchable biofuel cell with enzyme-modified conductive textiles.* Biosensors and Bioelectronics, 2015. **74**: p. 947-952.

50.   *Scanning Electron Microscope.* [cited 2018 September 29th];Available from: https://centers.njit.edu/york/analysis/electron-microscope.php.

51.   Cialla, D., et al., *Surface-enhanced Raman spectroscopy (SERS): progress and trends.* Analytical and Bioanalytical Chemistry, 2012. **403**(1): p. 27-54.

52.   Schlücker, S., *Surface-Enhanced Raman Spectroscopy: Concepts and Chemical Applications.* Angewandte Chemie International Edition, 2014. **53**(19): p. 4756-4795.

53.   Yuan, H., et al., *Spectral characterization and intracellular detection of Surface-Enhanced Raman Scattering (SERS)-encoded plasmonic gold nanostars.* Journal of Raman Spectroscopy, 2013. **44**(2): p. 234-239.

54.   Hrelescu, C., et al., *Single gold nanostars enhance Raman scattering.* Applied Physics Letters, 2009. **94**(15): p. 153113.

55.   *Raman Microscope*. [cited 2018 September 29th]; Available from: https://centers.njit.edu/york/analysis/raman-microscope.php.

56.   Wu, Z.-S., et al., *Gold colloid-bienzyme conjugates for glucose detection utilizing surface-enhanced Raman scattering.* Talanta, 2006. **70**(3): p. 533-539.

57.   Lin, X.-M., et al., *Surface-enhanced Raman spectroscopy: substrate-related issues.* Analytical and Bioanalytical Chemistry, 2009. **394**(7): p. 1729-1745.

58.   Iijima, S., *Helical microtubules of graphitic carbon.* Nature, 1991. **354**(6348): p. 56.

59.   Iijima, S. and T. Ichihashi, *Single-shell carbon nanotubes of 1-nm diameter.* Nature, 1993. **363**(6430): p. 603.

60.   Prasek, J., et al., *Methods for carbon nanotubes synthesis.* Journal of Materials Chemistry, 2011. **21**(40): p. 15872-15884.

61.   Dresselhaus, M., G. Dresselhaus, and R. Saito, *Physics of carbon nanotullbes.* Carbon, 1995. **33**: p. 883-891.

62.   Das, S., *A review on Carbon nano-tubes-A new era of nanotechnology.* International Journal of Emerging Technology and Advanced Engineering, 2013. **3**(3): p. 774-783.

63.   Ribeiro, B., et al., *Carbon nanotube buckypaper reinforced polymer composites: a review.* Polímeros, 2017. **27**(3): p. 247-255.

64.   Krätschmer, W., et al., *Solid C60: a new form of carbon.* Nature, 1990. **347**(6291): p. 354.

65.   Arora, N. and N. Sharma, *Arc discharge synthesis of carbon nanotubes: Comprehensive review.* Diamond and Related Materials, 2014. **50**: p. 135-150.

66.   Zhao, X., et al., *Morphology of carbon nanotubes prepared by carbon arc.* Japanese Journal of Applied Physics, 1996. **35**(8R): p. 4451.

67.   Zhao, X., et al., *Preparation of high-grade carbon nanotubes by hydrogen arc discharge.* Carbon, 1997. **35**(6): p. 775-781.

68.   Zhao, X., et al., *Morphology of carbon allotropes prepared by hydrogen arc discharge.* Journal of crystal growth, 1999. **198**: p. 934-938.

69.   Shimotani, K., et al., *New synthesis of multi-walled carbon nanotubes using an arc discharge technique under organic molecular atmospheres.* Applied Physics A, 2001. **73**(4): p. 451-454.

70.   Bethune, D., et al., *Cobalt-catalysed growth of carbon nanotubes with single-atomic-layer walls.* Nature, 1993. **363**(6430): p. 605-607.

71.   Guo, T., et al., *Catalytic growth of single-walled manotubes by laser vaporization.* Chemical Physics Letters, 1995. **243**(1-2): p. 49-54.

72.   Choudhary, V., B. Singh, and R. Mathur, *Carbon nanotubes and their composites*, in Syntheses and Applications of Carbon Nanotubes and Their Composites. 2013, InTech.

73.   Endo, M., et al., *The production and structure of pyrolytic carbon nanotubes (PCNTs).* Journal of Physics and Chemistry of Solids, 1993. **54**(12): p. 1841-1848.

74.   Palizdar, M., et al., *Investigation of Fe/MgO catalyst support precursors for the chemical vapour deposition growth of carbon nanotubes.* Journal of Nanoscience and Nanotechnology, 2011. **11**(6): p. 5345-5351.

75.   Tomie, T., et al., *Prospective growth region for chemical vapor deposition synthesis of carbon nanotube on C–H–O ternary diagram.* Diamond and Related Materials, 2010. **19**(11): p. 1401-1404.

76.   He, D., et al., *Growth of carbon nanotubes in six orthogonal directions on spherical alumina microparticles.* Carbon, 2011. **49**(7): p. 2273-2286.

77.   Shirazi, Y., et al., *Effects of different carbon precursors on synthesis of multiwall carbon nanotubes: Purification and Functionalization.* Applied Surface Science, 2011. **257**(16): p. 7359-7367.

78.   Khan, W., R. Sharma, and P. Saini, *Carbon nanotube-based polymer composites: synthesis, properties and applications*, in Carbon Nanotubes-Current Progress of their Polymer Composites. 2016, InTech.

79.   Feng, J.-M., et al., *One-step fabrication of high quality double-walled carbon nanotube thin films by a chemical vapor deposition process.* Carbon, 2010. **48**(13): p. 3817-3824.

80.   Li, G., *Synthesis of well-aligned carbon nanotubes on the NH 3 pretreatment Ni catalyst films.* Russian Journal of Physical Chemistry A, 2010. **84**(9): p. 1560-1565.

81.   Liu, Z., et al., *Aligned, ultralong single-walled carbon nanotubes: from synthesis, sorting, to electronic devices.* Advanced Materials, 2010. **22**(21): p. 2285-2310.

82.   Flahaut, E., C. Laurent, and A. Peigney, *Catalytic CVD synthesis of double and triple-walled carbon nanotubes by the control of the catalyst preparation.* Carbon, 2005. **43**(2): p. 375-383.

83.   Xiang, X., et al., *Co-based catalysts from Co/Fe/Al layered double hydroxides for preparation of carbon nanotubes.* Applied Clay Science, 2009. **42**(3-4): p. 405-409.

84.   Lyu, S.C., et al., *High-quality double-walled carbon nanotubes produced by catalytic decomposition of benzene.* Chemistry of Materials, 2003. **15**(20): p. 3951-3954.

85.   Zhang, D., et al., *Preparation and desalination performance of multiwall carbon nanotubes.* Materials Chemistry and Physics, 2006. **97**(2-3): p. 415-419.

86.   Hu, L., D.S. Hecht, and G. Gruner, *Carbon nanotube thin films: fabrication, properties, and applications.* Chemical Reviews, 2010. **110**(10): p. 5790-5844.

87.   Gooding, J.J., *Nanostructuring electrodes with carbon nanotubes: A review on electrochemistry and applications for sensing.* Electrochimica Acta, 2005. **50**(15): p. 3049-3060.

88.   Fuchsberger, K., et al., *Multiwalled Carbon-Nanotube-Functionalized Microelectrode Arrays Fabricated by Microcontact Printing: Platform for Studying Chemical and Electrical Neuronal Signaling.* Small, 2011. **7**(4): p. 524-530.

89.   Hughes, M., et al., *Electrochemical Capacitance of a Nanoporous Composite of Carbon Nanotubes and Polypyrrole.* Chemistry of Materials, 2002. **14**(4): p. 1610-1613.

90.   Holzinger, M., A. Le Goff, and S. Cosnier, *Carbon nanotube/enzyme biofuel cells.* Electrochimica Acta, 2012. **82**: p. 179-190.

91.   *Carbon Nanotube TEM Image*. 03/29/2017 [cited 2019 Feburary 23th];
       Available from: https://www.nano-lab.com/nanotube-image3.html.

92.   *Carbon Nanotube Image with Low Magnification*. [cited 2019 Feburary 23th];
       Available from: https://www.nano-lab.com/nanotube-image2.html.

93.   *Multi wall Carbon nanotube Raman data* [cited 2019 Feburary 23th];Available
       from: https://sep.yimg.com/ty/cdn/nanolab2000/Raman-
       PD15L520.pdf?t=1545172281&.

94.   Gao, F., O. Courjean, and N. Mano, *An improved glucose/O_2 membrane-less
       biofuel cell through glucose oxidase purification.* Biosensors and Bioelectronics,
       2009. **25**(2): p. 356-361.

95.   Gao, F., et al., *Engineering hybrid nanotube wires for high-power biofuel cells.*
       Nature Communications, 2010. **1**: p. 2.

96.   Palmore, G.T.R. and H.-H. Kim, *Electro-enzymatic reduction of dioxygen to
       water in the cathode compartment of a biofuel cell.* Journal of Electroanalytical
       Chemistry, 1999. **464**(1): p. 110-117.

97.   Campbell, E., et al., *Enzymatic biofuel cells utilizing a biomimetic cofactor.*
       Chemical Communications, 2012. **48**(13): p. 1898-1900.

98.   Durand, F., et al., *Designing a highly active soluble PQQ–glucose
       dehydrogenase for efficient glucose biosensors and biofuel cells.* Biochemical
       and Biophysical Research Communications, 2010. **402**(4): p. 750-754.

99.   Holland, J.T., et al., *Engineering of glucose oxidase for direct electron transfer
       via site-specific gold nanoparticle conjugation.* Journal of the American
       Chemical Society, 2011. **133**(48): p. 19262-19265.

100.   Armstrong, F.A. and G.S. Wilson, *Recent developments in faradaic
       bioelectrochemistry.* Electrochimica Acta, 2000. **45**(15-16): p. 2623-2645.

101.   Gregg, B.A. and A. Heller, *Cross-linked redox gels containing glucose oxidase
       for amperometric biosensor applications.* Analytical Chemistry, 1990. **62**(3): p.
       258-263.

102.   Willner, B., E. Katz, and I. Willner, *Electrical contacting of redox proteins by
       nanotechnological means.* Current Opinion in Biotechnology, 2006. **17**(6): p.
       589-596.

103.   Akers, N.L., C.M. Moore, and S.D. Minteer, *Development of alcohol/O_2 biofuel
       cells using salt-extracted tetrabutylammonium bromide/Nafion membranes to*

immobilize dehydrogenase enzymes. Electrochimica Acta, 2005. **50**(12): p. 2521-2525.

104.   Klotzbach, T., et al., *Effects of hydrophobic modification of chitosan and Nafion on transport properties, ion-exchange capacities, and enzyme immobilization.* Journal of Membrane Science, 2006. **282**(1-2): p. 276-283.

105.   Moore, C.M., et al., *Improving the environment for immobilized dehydrogenase enzymes by modifying Nafion with tetraalkylammonium bromides.* Biomacromolecules, 2004. **5**(4): p. 1241-1247.

106.   Zebda, A., et al., *Mediatorless high-power glucose biofuel cells based on compressed carbon nanotube-enzyme electrodes.* Nature Communications, 2011. **2**: p. 370.

107.   Zhong, Q., *Conventional and Flexible Biofuel Cells with Pressure-Fabrication of Bioelectrodes.* 2015.

108.   Milton, R.D., et al., *Hydrogen peroxide produced by glucose oxidase affects the performance of laccase cathodes in glucose/oxygen fuel cells: FAD-dependent glucose dehydrogenase as a replacement.* Physical Chemistry Chemical Physics, 2013. **15**(44): p. 19371-19379.

109.   Palmore, G.T.R., et al., *A methanol/dioxygen biofuel cell that uses NAD+-dependent dehydrogenases as catalysts: application of an electro-enzymatic method to regenerate nicotinamide adenine dinucleotide at low overpotentials.* Journal of Electroanalytical Chemistry, 1998. **443**(1): p. 155-161.

110.   Arechederra, R.L., B.L. Treu, and S.D. Minteer, *Development of glycerol/O_2 biofuel cell.* Journal of Power Sources, 2007. **173**(1): p. 156-161.

111.   Zhu, Z., et al., *A high-energy-density sugar biobattery based on a synthetic enzymatic pathway.* Nature Communications, 2014. **5**: p. 3026.

112.   McKee, D.W., *Catalytic decomposition of hydrogen peroxide by metals and alloys of the platinum group.* Journal of Catalysis, 1969. **14**(4): p. 355-364.

113.   El-Deab, M.S., F. Kitamura, and T. Ohsaka, *Poisoning effect of selected hydrocarbon impurities on the catalytic performance of Pt/C catalysts towards the oxygen reduction reaction.* Journal of The Electrochemical Society, 2013. **160**(6): p. F651-F658.

114.   Zamel, N. and X. Li, *Effect of contaminants on polymer electrolyte membrane fuel cells.* Progress in Energy and Combustion Science, 2011. **37**(3): p. 292-329.

115.   Miyake, T., et al., *Flexible, layered biofuel cells.* Biosensors and Bioelectronics, 2013. **40**(1): p. 45-49.

116.   Villarrubia, C.W.N., et al., *Practical electricity generation from a paper based biofuel cell powered by glucose in ubiquitous liquids.* Electrochemistry Communications, 2014. **45**: p. 44-47.

117.   Turkevich, J., *Colloidal gold. Part II.* Gold bulletin, 1985. **18**(4): p. 125-131.

118.   Frens, G., *Controlled nucleation for the regulation of the particle size in monodisperse gold suspensions.* Nature Physical Science, 1973. **241**(105): p. 20.

119.   Venkateswaran, S., *Raman spectrum of hydrogen peroxide.* Nature, 1931. **127**(3202): p. 406.

120.   Qi, G., et al., *Glucose oxidase probe as a surface-enhanced Raman scattering sensor for glucose.* Analytical and Bioanalytical Chemistry, 2016. **408**(26): p. 7513-7520.

121.   Wu, Z., et al., *N8− polynitrogen stabilized on multi-wall carbon nanotubes for oxygen-reduction reactions at ambient conditions.* Angewandte Chemie, 2014. **126**(46): p. 12763-12767.